Proceedings of the Institution of Mechanical Engineers, Part G: Journal of Aerospace Engineering, 2006, Volume 220, Number 2, Pages 61-83

A nonlinear unsteady aerodynamic model for insect-like flapping wings in the hover: Part I. Methodology and analysis

S A Ansari* R Żbikowski† K Knowles‡

Nomenclature

Latin Alphabet

a	location of pitch axis w.r.t. mid-chord
A_i	quasi-steady components of circulation ($i = 1 \ldots 11$), m^2/s
c	wing section chord length, m
$\mathcal{D}$	horizontal drag force orthogonal to gravity, N
$\mathcal{F}$	complex force, N
$\boldsymbol{F}$	force vector, N
h	heave displacement, m
$\dot{h}$	heave velocity, m/s
$\mathcal{I}$	complex impulse, Ns
$\mathcal{I}_m$	moment of impulse, Nms
$\Im$	imaginary part of
$\boldsymbol{I}$	impulse vector, Ns
$\boldsymbol{I_m}$	moment of impulse vector, Nms
l	lunge displacement, m

*Post-Doctoral Research Officer, *Corresponding author email:* s.a.ansari@cranfield.ac.uk

†Principal Research Officer

‡Head, Aeromechanical Systems Group

$\dot{l}$	lunge velocity, m/s
$\mathcal{L}$	vertically upwards lift force parallel to gravity, N
$\mathcal{M}$	moment about wing pitch axis, Nm
$\boldsymbol{M}$	moment vector, Nm
p	pressure, Pa
q	complex velocity, m/s
$\boldsymbol{q}$	velocity vector, m/s
r	radial distance from centre, m
R	radius of circle in $\mathcal{Z}$-plane, m
$\Re$	real part of
t	time, s
u	x-component of velocity, m/s
U_∞	freestream velocity, m/s
v	y-component of velocity, m/s
v_r	radial component of velocity, m/s
v_θ	circumferential component of velocity, m/s
x	real-axis coordinate in circle ($\mathcal{Z}$) plane, m
y	imaginary-axis coordinate in circle ($\mathcal{Z}$) plane, m
$\mathcal{Z}$	complex coordinates in circle plane ($= x + \imath y$), m

Greek Symbols

α	angle of attack, rad
$\dot{\alpha}$	pitch rate, rad/s
β	stroke-plane angle, rad
γ	vorticity, m/s
Γ	circulation, m^2/s

ϵ	(complex) shape parameter
ζ	complex coordinates in physical plane (= $\xi + \imath\eta$), m
η	imaginary-axis coordinate in physical (ζ) plane, m
θ	angle along circle in $\mathcal{Z}$-plane
$\imath$	complex $\imath$ (= $\sqrt{-1}$)
ξ	real-axis coordinate in physical (ζ) plane, m
π	circle constant
ρ	fluid density, kg/m^3
σ	aerofoil camber parameter, m
ς	dummy variable
τ	aerofoil thickness parameter, m
φ	velocity potential, m^2/s
ψ	stream function, m^2/s
Ω	complex potential, m^2/s

Subscripts/Superscripts/Notation

A_0	quasi-steady component
A_1	apparent-mass component (for forces and moments)
	or, wake-induced component (for vorticity and circulation)
A_2	wake-induced (and LEV-induced) component
A_3	wake (and LEV) component
A_{lv}	leading-edge vortex
A_{wk}	trailing-edge wake
$\check{A}$	rotating coordinate system
$\hat{A}$	translating coordinate system
$\tilde{A}$	inertial coordinate system

$\overline{A}$	complex conjugate of
$\boldsymbol{A}$	vector
$\dot{A}$	first derivative w.r.t. time, s^{-1}

Abbreviations/Acronyms

2-D	two-dimensional, planar
3-D	three-dimensional, spatial
FMAV	flapping-wing micro air vehicle
CFD	computational fluid dynamics
LEV	leading-edge vortex
MAV	micro air vehicle
w.r.t.	with respect to

1 Introduction

The need for small, intelligent, reconnaissance robots that are capable of discreetly penetrating into confined spaces such as shafts and tunnels, and manoeuvring in them, is the motivation behind this work. Agile flight inside buildings, stairwells, shafts and tunnels is also of significant military and civilian value. Such *micro air vehicles* (MAVs) show particular promise in so-called D^3—dull, dirty and dangerous—environments.

Current unmanned aerial vehicles are too large to achieve this and research has concluded that insect-like flapping flight is the optimum way to fulfil this capability [1–3]—fixed wing aircraft do not have the required low speed agility and miniature helicopters are noisy and inefficient. The unique flight envelope dictated by MAV requirements strongly favours insect-like flapping-wing propulsion [ibid.]; hence our interest in modelling this flight regime.

Hover is considered here mainly because of its simplicity; the complication of including a freestream flow (as in forward or climbing flight) is avoided. Further, as noted by [4], hover is also the most costly in terms of power requirement. A vehicle designed to hover is, therefore, likely to have sufficient power for forward flight. Flight control during the transition from hover to forward flight, however, is always a challenge for hovering vehicles so adequate power is not a sufficient guarantee of forward-flight capability.

The overall aim is to develop a model for determining performance (lift, thrust and aerodynamic moment) characteris-

tics for an insect-like flapping wing in the hover. With this information, wing-design guidelines for a flapping wing MAV (or FMAV) may be proposed.

This paper is organised as follows. In § 1, the flapping-wing problem is introduced by considering the wing kinematics of insects and the associated aerodynamic phenomena. This is followed by a brief review of current analytical work on insect flight aerodynamics. The methodology behind the aerodynamic modelling of insect-like flapping wings used in this paper is discussed in § 2. The details of the model are explained together with the underlying assumptions. The main analysis is presented in § 3 where the problem is divided into two—the 2-D modelling framework and its extension to 3-D. The calculation of forces and moments on the flapping wing is also included in this section. Finally, the paper concludes with § 4 where a summary of the main findings from this work are presented.

This is the first of a two-part paper [5, 6]. The theory behind the aerodynamic model being proposed is developed here and its implementation is discussed in the second part of the paper (referred to as Part II in the text that follows). Together, these two papers describe a suitable aerodynamic model for insect-like hovering flapping flight.

1.1 Flapping-Wing Problem

Before the problem of insect-like flapping can be analysed, an understanding of the wing kinematics and the associated aerodynamic phenomena are essential.

1.1.1 Wing Kinematics

The availability of high-speed photography has enabled reasonably good descriptions of the kinematics of insect wings [7–9]. There exist in nature a vast variety of insects, each with either one or two pairs of wings. We restrict ourselves to one pair of wings and, in particular, to Diptera which are two-winged flies, e.g. the fruit fly Drosophila, and are excellent flyers. The description below is for such an insect. The overall flapping motion is similar to the sculling motion of the oars on a rowboat, consisting essentially of three component motions—sweeping (fore and aft), heaving (or plunging, up and down) and pitching (changing incidence). Flapping frequency is typically in the 5–200 Hz range.

The wing motion can be divided broadly into two phases—*translational* and *rotational*. The translational phase consists of two halfstrokes—the *downstroke* and the *upstroke* (see Figure 1). The downstroke refers to the motion of the wing from its rearmost position to its foremost position, relative to the body. The upstroke describes the return cycle. At either end of the halfstrokes, the rotational phases come into play—*stroke reversal* occurs, whereby the wing rotates rapidly and reverses direction for the subsequent halfstroke. During this process, the morphological lower surface becomes the upper

surface and the leading-edge always leads (Figure 1).

The path traced out by the wing tip (relative to the body) during the wing stroke is similar to a figure-of-eight on a spherical surface (see Figure 2) as the wing semi-span is constant. The wing flaps back and forth about a roughly constant plane called the *stroke plane* (analogous to the tip-path-plane for rotorcraft). The stroke plane is inclined to the horizontal at the *stroke-plane angle* β (Figure 2).

During a halfstroke, the wing accelerates to a roughly constant speed around the middle of the halfstroke, before slowing down to rest at the end of it. The velocity during the wingbeat cycle is, therefore, non-uniform and for hover, in particular, the motion of the wing tip does not vary dramatically from a pure sinusoid [7]. Wing pitch also changes during the halfstroke, increasing gradually as the halfstroke proceeds. On average, the angle of attack during a halfstroke is about 35° at the 70%-span position [ibid.] and typical stroke lengths are of the order of 3–5 wing chords [10].

1.1.2 Aerodynamic Phenomena

The flow associated with insect flapping flight is incompressible, laminar, unsteady and occurs at low Reynolds numbers. Despite their short stroke lengths and small Reynolds numbers, insect wings generate forces much higher than their quasi-steady equivalents due to the presence of a number of unsteady aerodynamic effects. Under steady-state conditions, the high angles of attack used by flapping insect wings would normally stall a wing and give deteriorated aerodynamic characteristics. By contrast, insect wings continue to produce favourable forces even in these extreme conditions.

In 1996, Ellington et al made the remarkable discovery of the *leading-edge vortex* (LEV) on the wings of a scaled-up model of the hawkmoth Manduca sexta [11]. More experiments further verified their discovery [12–14]. Although the leading-edge vortex had been observed in earlier experiments [15–19] it was not until then that it received proper recognition for insect flight.

Ellington et al reported that the leading-edge vortex, which persisted through each halfstroke, existed on the wings and proposed that it was responsible for the augmented lift forces. The overall structure of the leading-edge vortex has been likened to that observed on low-aspect-ratio delta wings [13, 15]; it is produced and fed by a leading-edge separation.The augmented lift is similarly analogous to the vortex lift on delta wings. The leading-edge vortex starts close to the wing root and spirals towards the tip where it coalesces with the tip vortex and convects into the trailing wake [11]. Although dynamic stall has been suggested as a possible mechanism for the origin of the leading-edge vortex [e.g. 20, 21] , this is unlikely [22] since a dynamic-stall vortex breaks away almost immediately and rapidly convects as soon as the wing translates [23].

The leading-edge vortex has been seen on the wings of both large insects [11] and small ones [24]. Liu et al found that due to the presence of the leading-edge vortex, the wings of a hovering hawkmoth were able to generate vertical forces up to about 40% greater than required to support its weight [25]. The leading-edge vortex is, therefore, fundamental in explaining the large forces generated by flapping wings.

Recent experiments by Dickinson et al [26, 27] on a dynamically-scaled mechanical model of the tiny fruit fly Drosophila melanogaster have also revealed the presence of a strong bound leading-edge vortex. However, only weak spanwise spiralling was observed (unlike for the hawkmoth above), prompting them to conclude that the precise flow structure of the leading-edge vortex depends critically on Reynolds number.

As flapping wings move through the air, they encounter *apparent mass* forces arising from the mass of surrounding air also set in motion due to the wing movement. The high accelerations and rapid stroke reversals make these forces significant and they have to be accounted for.

Due to the repeated accelerations of the wing and the brevity of the half-strokes, starting vortices are created and remain in the vicinity of flapping wings and have a hindering effect on the growth of lift on the wings—the so-called *Wagner effect* [21].

In hover and slow forward flight, the flapping wings are likely to be affected by the *returning wake* from previous wingbeats. Depending on the particular flight conditions, this wake interaction may be either beneficial or detrimental. Dickinson detected large forces that could not be explained by either the translational or the rotational motions of the wing and attributed them to wake capture [9, 28].

All of the above effects need to be incorporated into any model aimed at representing the flapping-wing problem.

1.2 Analytical Work on Insect Flight Aerodynamics

Whereas insects and their flight have been widely discussed, aerodynamic analysis of their flapping-wing flight has received relatively little attention until recently [29–31]. After earlier work in this area by Osborne [32], the first major contribution is usually attributed to Pringle [33]. Both of these works were based on quasi-steady models — the instantaneous forces on the flapping wing were assumed to be equivalent to those for steady flight at the same instantaneous velocity and angle of attack.

Following on from the elucidative work of Weis-Fogh [4, 34] on insect flight mechanisms and a basic quasi-steady treatment (actuator-disk momentum theory and blade-element analysis) of some aspects of their flight, research into the aerodynamics of insect flapping flight was rejuvenated by Ellington's seminal work in the 1980s [7, 10, 35–38]. Although

his work still did not step out very far from quasi-steady models (momentum and blade-element methods), Ellington strongly speculated about the presence of unsteady mechanisms and his work led to further study in this area. The nature of the 'unsteadiness' was yet unclear.

Confirmation of the key rôle of the leading-edge vortex by Ellington et al led to the most complete description of insect-wing flapping flow yet [11]. The flow is now understood to comprise two components— *attached* flow due to freestream flow over the wing and that due to the unsteady motion of the wing (sweeping, heaving and pitching), and *separated* flow in the form of wakes shed from both leading and trailing edges.

Until recently, the closest case to flapping wings considered for aerodynamic analysis was the problem of wings in severe unsteady manoeuvres [e.g. 39, 40] . Benson [41] and Lam [42] presented a particularly comprehensive technique based on the classical circulation approach of von Kármán & Sears [43] but by dropping a number of linearising assumptions in their analyses. They considered the case of 2-D flat plate wing executing severe unsteady motion.

Żbikowski [22] proposed two different approaches to analytical modelling of the insect-like flapping-wing problem—the velocity-potential and circulation approaches. Pedersen [44] used the velocity-potential approach to devise a method for predicting the forces on a flapping wing for given kinematics and found good agreement for lift forces. His model used a combination of the approaches of Wagner [45], Theodorsen [46] and Loewy [47] for attached flow together with a form of the leading-edge-suction analogy of Polhamus [48] for vortex lift. Whereas the model predicted lift forces with reasonable accuracy, drag (or thrust) data yielded unsatisfactory comparison.

Minotti [49] produced a circulation-based analysis for insect-like flapping wings. He divided the problem into the trailing-edge wake and the leading-edge vortex, and summed their respective influences. The change in bound circulation with time was computed using the method of Graham [50] whereby the starting vortex was modelled as a point vortex connected to the trailing edge via a branch cut. The leading-edge vortex was represented by a single 'fixed' point vortex at a position that gave best agreement with the experimental data of Sane & Dickinson [27]. The placement of the leading-edge vortex was somewhat arbitrary in that, in certain instances (around stroke reversals), it was placed much closer to the trailing edge than the leading edge, depending on a specially-defined incidence velocity.

Jones, Platzer *et al* have investigated the propulsive properties of aerofoils flapping in heaving oscillation—the so-called Knoller-Betz effect— both theoretically and experimentally [51–55]. The wing flapping motion in their investigations was, however, not insect-like.

In 1994, Dickinson carried out 2-D experiments on insect-like flapping-wing motion and investigated the effects on lift of several kinematics parameters [28]. Later 3-D experiments by Sane & Dickinson using a Drosophila-type wing

revealed similar findings [56]. This similarity between their 2-D and 3-D results forced speculation that results for a 3-D flow regime could indeed be derived from an extension of 2-D results (using, for example, blade-element theory) at least for the order of Reynolds number in question ($Re \approx 200 - 300$ based on mean chord and tip velocity).

Wang has also been tackling the problem of insect-flight aerodynamics but from a CFD point of view [57, 58]. Using Navier-Stokes calculations, she has studied the flow associated with accelerating flat plates with application to flapping-wing flight [59, 60]. Similarly, using both an inviscid model and CFD methods, [61] analysed the flow past an accelerating flat plate at fixed incidence angles.

More recently, Jones [62] considered the unsteady separated flow of an inviscid fluid around a moving flat plate. By assuming the premise that the flow consisted of a sheet of bound vorticity and two free vortex sheets (one each emanating from the leading and trailing edges), he used a boundary-integral method to represent and solve for the velocity field. His numerical method, however, could not handle the wing interacting with its own wake, which is a fundamental drawback in terms of insect-like flapping-wing applications where such interactions are ubiquitous. Further, the occurence of a 'numerical event' prevented the time-integration of the evolution equations beyond a certain finite time [62, § 7.1], presenting another limitation. Zdunich [63] arrived at similar results for the unsteady separated flow around a thin aerofoil but without recourse to complex algebra.

The poor quality of drag prediction from the model of Pedersen [44] (see above) identified the need for an improved method that would still incorporate the unsteady aerodynamic effects identified above (as did Pedersen) but give better prediction of forces. The circulation approach proposed by Żbikowski [22] was chosen for this purpose and has been developed here with significant modifications and improvements. An added advantage of this approach is the automatic generation of flow visualisation. The resulting modelling approach forms the basis of this two-part paper.

The core of the present work, therefore, is the theoretical development of an analytical, inviscid and nonlinear unsteady aerodynamic model of insect-like flapping wings in the hover. The method is circulation-based and quasi-three-dimensional in nature. Insect-like kinematics and wing geometry are used to generate force (and moment) data and flow visualisation. As will be shown in Part II, this approach shows remarkable agreement with existing experimental data both in terms of flowfield representation and force prediction; see [6].

2 Methodology

The aerodynamic modelling of flapping wings poses its own unique set of problems. The extreme manoeuvres of the wings expose a whole new flow regime, very different from that observed in conventional aircraft flight. Reynolds numbers for insect flight are also low, typically of the order of a few thousand. Viscosity becomes more important and drives some salient flow features not expected from conventional aerodynamics.

As noted by Thwaites, any new theory must take into account as far as possible what appear to be the most important physical characteristics [64, p. 512]. Thwaites further noted that for wing aerodynamics the positions of the separation lines, in particular, must be taken into account. Therefore, those properties and flow features that need to be represented in a model for insect-like flapping wings must first be identified.

From the review presented in § 1 above, the following conclusions can be drawn. The flow associated with insect-like flapping comprises two components— *attached* and *separated* flow. The attached flow on the aerofoil refers to all flow characteristics associated with the *freestream* flow on the aerofoil as well as the effects of *unsteady motions* (sweeping, heaving and pitching). In insect-like flapping wings, flow separation is usually observed at both leading and trailing edges due to the high angles of attack and the severity[1] of the kinematics. These 'wakes' affect the forces (and moments) generated by the wing due to their interaction with the wing. The back and forth motion of the wings also gives rise to effects associated with wake re-entry. The *leading-edge vortex* is bound to the wing for most of the duration of each halfstroke and flow remains more or less attached in all other regions of the wing. The *trailing-edge wake* leaves smoothly from the trailing edge (except perhaps during stroke reversals when the smooth-flow condition may not hold). All of the above features must be included in any representative model.

With this flow 'picture' in mind, Żbikowski proposed a circulation-based approach for solving the flapping-wing problem [22]. The problem may be decomposed into attached and separated flow, and the overall effect obtained by summing the individual contributions. It is based on the original approach of von Kármán & Sears [43] together with the nonlinear extensions proposed by McCune et al [65–67]. This is broadly the approach used in the current work albeit with further significant extensions.

[1] Severity implies rapidity and complexity in this case.

2.1 Model

2.1.1 Physical Aspects

A blade-element-type method is used whereby flow is analysed in chord-wise 2-D cross-planes and the combined effect obtained by integrating for all wing sections. Because the wing motion is rotary, the velocities and distances travelled increase radially from root to tip. This approach is described here as quasi-3-D. Two physical properties that are a consequence of this rotary motion are taken into account and are described below.

Radial Chord An insect-like flapping wing bears resemblance to a rotorcraft wing in that velocities increase radially from root to tip. For wings of high aspect ratio, such as helicopter rotors, the ratio of blade area to disk area (the so-called *solidity*) is very small (about 7.5% for a rotor with blades of aspect ratio 17) and it is reasonable to assume that the blade elements are straight (i.e. normal to the rotor spar). In the case of flapping wings such as those of insects, solidity is much higher (about 39% for the hawkmoth used by Wakeling & Ellington [68] and 55% for the fruit fly scaled wing used by Birch & Dickinson [26]) and the straight-chord assumption is less tenable. Instead, the concept of a *radial chord* is more suitable where each section of the wing chord still 'sees' a normal incident velocity (Figure 3).

In the analysis that follows, all radial chords are computed with the wing lying flat as if at zero angle of attack α in a stroke plane at zero stroke-plane angle β. In reality, radial chords can be very complex, depending on instantaneous angle of attack and local incident velocity (which includes a spherical component due to the nature of the wing motion). For reasons of simplicity, however, the latter have been ignored so only one set of radial chords is used for a given problem.

Radial and Flat Cross-Planes A consequence of combining a blade-element method with the concept of radial chords discussed above is that consecutive wing sections lie in cylindrical cross-planes (see Figure 4(a)). In the approach used here, each cylindrical cross-plane is then 'unwrapped' into an equivalent flat cross-plane (Figure 4(b)) where the flow is then solved as a 2-D problem. This concept is met in differential geometry problems where the radial cross-plane would be referred to as a developable surface[2].

[2] A developable (or ruled) surface is one formed by motion of a straight line. Therefore, a cylindrical surface (as used here) is developable but a spherical one is not [69].

2.1.2 Aerodynamic Aspects

There exist a large number of fluid flows that are affected by viscosity to the first order and yet their motions do not show signs of restrictive amounts of viscous dissipation. Such flows may be treated as special cases of potential or irrotational flows [70], allowing them to be solved by well-known analytical methods.

In each 2-D section, the aerofoil is represented by a continuous distribution of bound vorticity[3]and the zero-through-flow condition is enforced, i.e. the local flow velocity always remains tangential to the aerofoil surface. Two wakes are shed in the form of free vortex sheets—one each emanating from the leading and trailing edges—which are also continuous distributions of vorticity. The flow is assumed to be entirely inviscid but the effects of viscosity are introduced indirectly in the form of flow separation and the Kutta-Joukowski condition at the points of inception of the wakes. Bound vorticity at the aerofoil surface arises from the shear flow there and, hence, is also a consequence of viscosity. As a result, the flow is irrotational everywhere except at the solid boundaries and in the free vortex sheets.

The flow is solved for using potential methods by satisfying the kinematic boundary conditions, the Kutta-Joukowski conditions at the wake-inception points and by requiring that the total circulation in a control volume enclosing the system must remain constant (Kelvin's law; see [72, § 33, p. 36]). More is said about these in the detailed analysis later (see § 3).

The exact nature of the leading-edge vortex found on insect flapping wings remains elusive. Whereas Ellington et al reported spanwise velocity in the leading-edge vortex [11], Dickinson et al observed no such entrainment [26, 27]. The current modelling framework cannot treat spanwise flow but this does not pose a problem because the only validation data available were provided by Dickinson [priv. comm.] who observed no such flow. Therefore, no interaction is assumed to exist between adjacent wing sections. Glauert [73, pp. 211–212] supported this view in his blade-element theory for propellers, although he did not completely discount the possibility of radial phenomena in the tip regions.

An extension of the previous assumption (no interference between adjacent sections) is that tip vortex effects are also ignored. The performance of the entire wing is obtained simply by summing the individual contributions of the constituent 2-D wing sections. The validity of this assumption was established a posteriori as the results were found to compare well with experimental data (see Part II). It would appear that the loss of lift (and thrust) due to 2-D vortex breakdown in the outboard sections of the wing is equivalent to the drop in lift (and thrust) that would be experienced in those regions due to tip-vortex effects.

[3]This property differentiates the method from panel methods where the aerofoil is divided into panels each with two *distinct* points— one for vortex position and one for collocation point [see Ref. 71, ch. 9].

2.1.3 Assumptions

While care has been taken to maintain generality and to keep simplifications to a minimum, a number of simplifying assumptions had to be made. These are summarised below.

- The wing is a thin, flat plate (zero thickness and camber).
- The wing is rigid (there is no flexion irrespective of the severity of the kinematics).
- The flow is entirely inviscid although viscosity is indirectly introduced in the form of the Kutta-Joukowski condition and flow separation at the sharp leading- and trailing-edges.
- The flow is irrotational (zero vorticity and incompressible) everywhere except at solid boundaries and in the distribution of wake vorticity.
- Radial chords are used to describe each wing section because, as a result of the rotary motion of the wing, each wing section sees a ‘curved’ oncoming velocity.
- Each radial chord is computed with the wing lying flat (in reality, radial chords are spherical in nature and vary with incidence and incident velocity).
- As a result of the radial chords, the wake is enclosed within cylindrical surfaces (whereas the wing motion is actually spherical and the wake is likely to have a much more complex form).
- No interaction is assumed between adjacent wing sections so that the combined effect is obtained simply by integrating along the span (the underlying assumption here is that spanwise variation in wing cross-section must be minimal).
- As a consequence of the previous assumption, any spanwise flow (as in, for example, the leading-edge vortex) is not modelled.
- Tip-vortex effects are ignored.
- No interference effects between two wings are considered so that the combined effect is obtained simply by doubling the results for one wing.
- Only the hover mode of flight is considered.
- Wing twist is ignored and the wing is assumed to have a common pitch axis for all wing sections.

- Laminar flow is assumed throughout on account of the low Reynolds numbers encountered in insect (and likely FMAV) flows.
- The effects of attached, separated and shed flows are linearly superposable (on the basis of the linearity of the Laplace equation).

2.1.4 Conformal Transformation

The crux of the current approach is the conformal mapping of a circle into a Joukowski-type aerofoil. In this way, a complicated problem in physical space is transformed into a simpler problem in transformed space. An important feature of such a transformation is that angles are preserved—the angle between a pair of lines remains unchanged through the transformation process. This property is essential so that the zero-through-flow condition, which requires that fluid flow be tangential to the aerofoil surface at all times, can be enforced correctly in the circle plane where it is being computed.

The simple case of flow around a 2-D circular cylinder (or circle, in the $\mathcal{Z}$-plane) is mapped into that around a Joukowski-type aerofoil (in the ζ-plane) using the following transformation

$$\zeta = \mathcal{Z} + \frac{(1-\epsilon)R^2}{\mathcal{Z}} + \frac{\epsilon R^3}{2\mathcal{Z}^2} \tag{1}$$

where

$$\epsilon = \frac{\tau - \imath\sigma}{R}$$

and where R is the radius of the circle, and τ and σ are thickness and camber parameters respectively. This form of conformal transformation was developed by McCune (see [41,42]) based on the rules presented by Karamcheti [74, ch. 14] whereby a whole range of Joukowski-type aerofoils could be defined while still maintaining the same corresponding circle in the $\mathcal{Z}$-plane.

The advantage of using this transformation is that the trailing edge is always at the point $\mathcal{Z} = R$ and that the circle is always centred at the origin. The latter enables use of *conjugate function theory* (see [75], Appendix A; see also [74] for full details) to calculate tangential or radial velocity components from each other (which will be essential as we will see later)[4]. Another advantage of this transformation is that a horizontal freestream velocity remains horizontal throughout—a rotation through the angle of attack is not required.

[4]For a conventional Joukowski transformation of the form $\zeta = \mathcal{Z} + \frac{R^2}{\mathcal{Z}}$, the centre of the circle is not necessarily at the origin in the $\mathcal{Z}$-plane and, hence, conjugate function theory cannot always be applied.

The usual laws of conformal transformation are observed so that the following relationships, in particular, hold for an aerofoil in the physical (ζ) plane transformed into a circle in the transformed ($\mathcal{Z}$) plane.

$$q(\zeta) = \frac{q(\mathcal{Z})}{\frac{\mathrm{d}\zeta}{\mathrm{d}\mathcal{Z}}} \qquad (q : \text{complex velocity}) \tag{2a}$$

$$\gamma(\zeta) = \frac{\gamma(\mathcal{Z})}{\frac{\mathrm{d}\zeta}{\mathrm{d}\mathcal{Z}}} \qquad (\gamma : \text{vorticity}) \tag{2b}$$

$$\Gamma(\zeta) = \Gamma(\mathcal{Z}) \qquad (\Gamma : \text{circulation}) \tag{2c}$$

In the case where $\tau = \sigma = 0$, the aerofoil shape parameter $\epsilon = 0$ and Equation 1 takes the more conventional form of the Joukowski transformation given in Footnote 4. In such a case, the aerofoil reduces to a flat plate with chord $c = 4R$. It may also be noted that τ and σ only *control* thickness and camber respectively; they are not the maximum thickness and maximum camber of the aerofoil per se.

In the subsequent analysis, extensive use is made of the complex variable and its properties [a detailed account can be found in Ref. 74, ch. 15]. Two-dimensional potential flow can be described conveniently by means of the Cauchy-Riemann equations which state the equivalence of velocity potential φ and stream function ψ in describing potential flows. For flows around a circle, polar velocity components are more useful and can easily be obtained using the conversion

$$u - \imath v = (v_r - \imath v_\theta)\, \mathrm{e}^{\imath\theta} \tag{3}$$

where (u, v) describe the Cartesian velocity components at the point (x, y), v_r and v_θ are the radial and circumferential velocity components at the same point respectively, and θ is the angular displacement measured at the origin. This relationship is employed later.

3 Analysis

In the analysis that follows, the aerofoil is represented by a continuous distribution of bound vortices that move with the aerofoil. The wakes that emanate at both leading and trailing edges are similarly continuous distributions of vortices but are free and move with the fluid. The advantage of conformal transformation is exploited so that all calculations are performed in the circle plane for simplicity. As necessary, the relevant elements are then converted into the physical plane where they have more meaning.

3.1 Two-dimensional Unsteady Analysis

Analysis of the flow around a flapping-wing aerofoil is described by means of a potential-flow method, incorporating observations from insect flight and relying heavily on the complex variable and conformal transformations discussed above[5]. Smith et al have noted that even flows with Reynolds numbers as low as $Re \approx 10000$ are inertia-dominated so that viscous effects should not be directly important in most of the flow field and, hence, potential methods can be employed [76]. Reynolds numbers for FMAV flows are likely to be in this region so potential methods are used here.

The flow around a 3-D flapping wing is treated in a quasi-3-D manner by adopting a blade-element-type approach. By assuming that the flow is inviscid and incompressible, the Navier-Stokes equations reduce to the Euler equation and potential-flow methods can be used. Further, the flow is assumed to be irrotational everywhere (except at solid boundaries and discontinuities in the wake). So in essence, the flow is solved for using Laplace's equation, which in complex-number notation requires that

$$\nabla^2(\varphi + \imath\psi) = 0$$

where φ is velocity potential and ψ is stream function. The nature of Laplace's equation means that the principle of superposition can be applied. This implies that the effects of various components contributing to the fluid motion may be computed separately and the overall effect obtained by taking their sum. This is the cornerstone of the current approach.

Nonlinearity in the model arises from the nature of the kernels of the integral equations developed (see Equations 22 and 25 later) and the fact that the shed wakes are not flat (unlike in small-perturbation theory). The overall formulation of the problem is still linear, thereby allowing superposition. Alternatively, because vorticity is no longer confined to bound vorticity on the wing but also appears in the surrounding flowfield (due to the two shed wakes), this approach also appeals to the Helmholtz decomposition [77] where the flowfield can be modelled as the superposition of a potential and a rotational field.

Although viscosity is generally ignored, its effects are included indirectly in the form of the Kutta-Joukowski condition, separation at the leading and trailing edges, and in the formation and shedding of vortices.

In our approach, the linearity of Laplace's equation is exploited to describe the flow associated with an insect-like flapping wing. The problem is subdivided into wake-free and wake-induced components (see Figure 5). The former subdivides further into effects due to *freestream* velocity and those due to the *unsteady motion* of the flapping wing itself.

[5]The analysis presented in this section is based on an approach similar to that used by Benson [41] and Lam [42] albeit with several extensions and modifications. All calculations presented were made from first principles and errors in the works of Benson and Lam have also been corrected.

Since these effects exclude any wake contribution, they are collectively termed the *quasi-steady* components.

The wake-induced components also further subdivide into the contributions of the *leading-edge vortex* and the *trailing-edge wake*. These components induce the remaining forces and moments on the wing and are henceforth referred to as the *unsteady* components. The unsteady nature of the whole problem makes each of the component contributions functions of time.

Each of these components is considered below. The vorticity and circulation developed by the aerofoil (and in the wake, where applicable) as a result of each of the components is calculated. These are later used to compute forces and moments. Dependence on time t is assumed throughout although it has been omitted from the notation on several occasions for reasons of clarity. As noted earlier, all analysis is performed in the circle ($\mathcal{Z}$) plane for simplicity.

Conventions and Coordinate Systems Before proceeding, a quick note on some of the conventions and coordinate systems used is appropriate. In the analysis that follows, circulation (and vorticity) is taken positive counterclockwise ($\circlearrowleft$). Moments are also taken positive counterclockwise.

Conventional rectangular coordinates are used so that the abscissa and ordinate point left to right and bottom to top respectively, and are orthogonal with respect to each other (see Figure 6). By default, the onset flow velocity is taken from left to right. Consequently, positive angle of attack and pitch rate are taken positive clockwise. Due to the unsteady flapping motion, the aerofoil may either point leftwards or rightwards depending on the instantaneous kinematics. When the aerofoil points rightwards, angle of attack exceeds 90°. The aerofoil has three degrees of freedom — lunge (horizontal perturbations), heave (vertical perturbations) and pitch (angular perturbations). Positive lunge is in the direction of the freestream flow (i.e. from left to right in Figure 6) and positive heave is upwards.

Four different Lagrangian coordinate systems are defined—*aerofoil*, *rotating*, *translating* and *inertial* (see Figure 6). The aerofoil coordinate system (ζ) is fixed at the centre[6] of the aerofoil and moves with it. The rotating coordinate system ($\check{\zeta}$) also moves with the aerofoil but is centred at the pitch axis of the aerofoil and is oriented with the aerofoil. When the pitch axis is at the centre of the aerofoil, the aerofoil and rotating axes coincide exactly.

The translating coordinate system ($\hat{\zeta}$) shares its origin with the rotating axes system but differs in that it remains horizontal (w.r.t. gravity) at all times. When the aerofoil is horizontal and the pitch axis is at its centre, the translating and aerofoil axes coincide. The inertial coordinate system ($\tilde{\zeta}$) remains fixed with respect to the Earth. For the wing sections, the origins of their respective inertial systems lie along the same radial line from root to tip, coinciding with the $\phi = 0$ line

[6]This is the geometric centre of the aerofoil and can be found by mapping the centre of the circle in the $\mathcal{Z}$-plane into the ζ-plane.

(ϕ being sweep angle; see Figure 4(a)).

The rotating coordinate system is used to describe the rotational motion of the aerofoil whereas the translating coordinate system describes its translational motion. Both these coordinate systems move with the aerofoil and are hence termed *aerofoil-inertia* systems.

3.1.1 Quasi-Steady Component

If an aerofoil with complex coordinates $\zeta = \xi + \imath\eta$ corresponds to the circle $\mathcal{Z} = R\,\mathrm{e}^{\imath\theta}$ (where R is radius and θ is angular displacement about its centre), then by Equation 1 the aerofoil coordinates are

$$\xi = 2R\cos\theta + \sigma\left(\sin\theta - \tfrac{1}{2}\sin 2\theta\right) - \tau\left(\cos\theta - \tfrac{1}{2}\cos 2\theta\right) \tag{4a}$$

$$\eta = \tau\left(\sin\theta - \tfrac{1}{2}\sin 2\theta\right) + \sigma\left(\cos\theta - \tfrac{1}{2}\cos 2\theta\right) \tag{4b}$$

These relations are employed later.

Freestream Component

The case for an aerofoil at an angle of attack α in a freestream flow is considered (Figure 7)[7]. Using the circle theorem [78, § 5.2], the complex potential of freestream flow of velocity U_∞ around the corresponding circle is

$$\Omega(\mathcal{Z}) = U_\infty\left(\mathcal{Z}\mathrm{e}^{-\imath\alpha} + \frac{R^2\mathrm{e}^{\imath\alpha}}{\mathcal{Z}}\right)$$

which differentiates to give the complex velocity, thus

$$q(\mathcal{Z}) = \frac{\mathrm{d}\Omega}{\mathrm{d}\mathcal{Z}} = U_\infty\left(\mathrm{e}^{-\imath\alpha} - \frac{R^2\mathrm{e}^{\imath\alpha}}{\mathcal{Z}^2}\right)$$

By using the substitution $\mathcal{Z} = R\mathrm{e}^{\imath\theta}$ on the circle and converting to polar coordinates using Equation 3, the circumferential (tangential) velocity can be obtained. For smooth flow at the trailing edge (i.e. at $\theta = 0$), the Kutta-Joukowski condition must be enforced there by adding a circulation Γ_k at the origin so that the circumferential velocity v_θ becomes

$$v_\theta(\theta)|_{fs} = -2U_\infty\sin(\theta - \alpha) + \frac{\Gamma_k}{2\pi R}$$

where the subscript $_{fs}$ refers to the freestream component, $\Gamma_k = -4\pi R U_\infty\sin\alpha$ and where α and, hence, Γ_k can be time-varying. The value of Γ_k is fixed in accordance with the Kutta-Joukowski condition by requiring $v_\theta = 0$ at $\theta = 0$. Assuming that no flow exists within the circle, the circumferential velocity at any point on the circle is equivalent to the vorticity

[7] Although there is no freestream velocity in hover, it has been included in the analysis for completeness.

there, thus

$$\gamma_0(\theta,t)|_{fs} = -2U_\infty\Big[\sin\theta - \alpha(t) + \sin\alpha(t)\Big] \tag{5}$$

from which the circulation is obtained by integration as

$$\Gamma_0(t)|_{fs} = -4\pi R U_\infty \sin\alpha(t) \tag{6}$$

As discussed previously (Equation 2c), circulation is preserved through a conformal transformation so that the expression above also gives the circulation around the aerofoil. The negative sign is a consequence of the convention used— positive circulation is taken counterclockwise (in the sense of increasing θ).

Unsteady Motion Component

The unsteady motion of the flapping-wing aerofoil disturbs the fluid around it. Because the wing is represented by a series of vortices, their strengths have to be adjusted so that the solid boundary condition is upheld. Therefore, in order to determine the bound vorticity (and circulation) due to this unsteady motion, the kinematic boundary condition must first be derived. This yields velocity components at the aerofoil surface which can then be used to derive expressions for vorticity (and circulation) as was done for the freestream component above.

The zero-through-flow condition requires that fluid does not penetrate the aerofoil surface and so the normal velocity at the surface must be zero, i.e. $v_n = 0$. Before such a condition can be derived, however, the instantaneous position of the aerofoil must be determined. The 2-D aerofoil has three degrees of freedom (see Figure 6)—pitch $(\alpha, \dot{\alpha})$, lunge $(l, \dot{l})$ and heave $(h, \dot{h})$ where the dot $(\dot{})$ means differentiation w.r.t. time. To enforce the zero-through-flow boundary condition at the surface of the aerofoil, the fluid velocity $(\tilde{u}, \tilde{v})$ and aerofoil kinematic velocity $(\tilde{u}_a, \tilde{v}_a)$ must be equal there. This condition is satisfied when

$$u = \dot{l}\cos\alpha - \dot{h}\sin\alpha + \eta\dot{\alpha} \tag{7a}$$

$$v = \dot{l}\sin\alpha + \dot{h}\cos\alpha - (\xi + a)\dot{\alpha} \tag{7b}$$

Equations 7 are the required zero-through-flow boundary conditions and must not be confused as conversions between coordinate systems[8]. The no-slip boundary condition on the solid-fluid interface cannot be enforced because viscosity has been neglected.

[8]This boundary condition can also be derived in an alternative way by defining the aerofoil surface as $\aleph(\xi,\eta,t) = 0$, equating the substantial derivative at the aerofoil surface to zero, thus $\mathrm{D}\aleph/\mathrm{D}t|_{us} = 0$, and then solving for u and v [see Ref. 75, Appendix C].

Now that the kinematic boundary condition for the unsteady motion of the aerofoil has been found (Equations 7), the circumferential (tangential) velocity on the corresponding circle needs to be derived. This in turn will yield vorticity which will then be used to compute the bound circulation around the aerofoil due to its unsteady motion.

The complex velocity at a point in the aerofoil (ζ) plane is given by

$$q(\mathcal{Z}) = u - \imath v \tag{8}$$

By combining Equations 2a and 3 with Equation 8, the velocity in the circle plane can be written in terms of that in the aerofoil plane thus

$$v_r - \imath v_\theta = (u - \imath v)\, \mathrm{e}^{\imath\theta} \frac{\mathrm{d}\zeta}{\mathrm{d}\mathcal{Z}} \tag{9}$$

Using the substitution $\mathrm{e}^{\imath\theta} \frac{\mathrm{d}\zeta}{\mathrm{d}\mathcal{Z}} = A + \imath B$, Equation 9 becomes

$$\begin{aligned} v_r - \imath v_\theta &= (u - \imath v)(A + \imath B) \\ &= (Au + Bv) + \imath (Bu - Av) \end{aligned} \tag{10a}$$

where

$$A = \frac{1}{R}\left[\tau(\cos\theta - \cos 2\theta) - \sigma(\sin\theta - \sin 2\theta)\right] \tag{10b}$$

$$B = \frac{1}{R}\left[2R\sin\theta - \tau(\sin\theta - \sin 2\theta) - \sigma(\cos\theta - \cos 2\theta)\right] \tag{10c}$$

The zero-through-flow boundary condition stated earlier (Equations 7) applies only to the component of velocity normal to the aerofoil surface—it makes no attempt to describe the tangential component. The values for u and v deduced above (Equations 7a and 7b respectively), therefore, only correspond to the component of velocity *normal* to the surface of the circle, i.e. v_r in Equation 10. Since u and v do not carry information about the component of velocity tangential to the surface, only the real parts of Equation 10a can be used, thus

$$v_r = Au + Bv \tag{11}$$

It is important to make the above distinction. Substituting from Equations 4, 7 and 10 into Equation 11 and rearranging gives

$$\begin{aligned} v_r(\theta, t)|_{us} = \frac{1}{R}\big(&A_1 \sin\theta + A_2 \sin 2\theta + A_3 \cos\theta + A_4 \cos 2\theta + A_5 \sin^2\theta + A_6 \cos^2\theta + A_7 \sin\theta\cos\theta \\ &+ A_8 \sin\theta \sin 2\theta + A_9 \sin\theta \cos 2\theta + A_{10} \cos\theta \sin 2\theta + A_{11} \cos\theta \cos 2\theta\big) \end{aligned} \tag{12}$$

where

$$
\begin{aligned}
A_1 &= -\sigma(\dot{l}\cos\alpha - \dot{h}\sin\alpha) + (2R-\tau)(\dot{l}\sin\alpha + \dot{h}\cos\alpha) + a(\tau-2R)\dot{\alpha} \\
A_2 &= \sigma(\dot{l}\cos\alpha - \dot{h}\sin\alpha) + \tau(\dot{l}\sin\alpha + \dot{h}\cos\alpha) - a\tau\dot{\alpha} \\
A_3 &= \tau(\dot{l}\cos\alpha - \dot{h}\sin\alpha) - \sigma(\dot{l}\sin\alpha + \dot{h}\cos\alpha) + a\sigma\dot{\alpha} \\
A_4 &= -\tau(\dot{l}\cos\alpha - \dot{h}\sin\alpha) + \sigma(\dot{l}\sin\alpha + \dot{h}\cos\alpha) - a\sigma\dot{\alpha} \\
A_5 &= -2R\sigma\dot{\alpha} \\
A_6 &= 2R\sigma\dot{\alpha} \\
A_7 &= 4R(\tau-R)\dot{\alpha} \\
A_8 &= R\sigma\dot{\alpha} \\
A_9 &= -\tfrac{1}{2}(\tau^2+\sigma^2+2R\tau)\dot{\alpha} \\
A_{10} &= \tfrac{1}{2}(\tau^2+\sigma^2-4R\tau)\dot{\alpha} \\
A_{11} &= -2R\sigma\dot{\alpha}
\end{aligned}
\tag{13}
$$

and the subscript $_{us}$ indicates contribution due to the unsteady aerofoil motion. To calculate vorticity (and hence, circulation) on the surface of the circle, the circumferential velocity v_θ must be known. This can be evaluated using the radial velocity (Equation 12) and applying conjugate function theory [see Ref. 75, Appendix A]. The transformation equation is

$$
v_\theta(\theta,t)|_{us} = -\frac{1}{2\pi}\oint_0^{2\pi} v_r(\varsigma,t)|_{us}\,\cot\left(\frac{\varsigma-\theta}{2}\right)\mathrm{d}\varsigma \tag{14}
$$

The right-hand side of Equation 14 features a principal value integral[9] which is solved by judicious use of the Glauert integrals to give

$$
\begin{aligned}
&\oint_0^{2\pi} v_r(\varsigma,t)|_{us}\left(\frac{\sin\theta+\sin\varsigma}{\cos\theta-\cos\varsigma}\right)\mathrm{d}\varsigma \\
&= \frac{2\pi}{R}\Big(A_1\cos\theta + A_2\cos2\theta - A_3\sin\theta - A_4\sin2\theta + A_5\sin\theta\cos\theta - A_6\sin\theta\cos\theta + A_7\sin\theta\cos\theta \\
&\qquad + A_8\sin\theta\cos2\theta - A_9\sin\theta\cos2\theta + A_{10}\cos\theta\cos2\theta - A_{11}\cos\theta\sin\theta\Big)
\end{aligned}
$$

The circumferential velocity can then be readily calculated as

$$
\begin{aligned}
v_\theta(\theta,t)\,|_{us} = \frac{1}{R}\Big[&-A_1\cos\theta - \left(A_2+\tfrac{1}{2}A_7\right)\cos2\theta + A_3\sin\theta + \left(A_4-\tfrac{1}{2}A_5+\tfrac{1}{2}A_6\right)\sin2\theta \\
&- A_8\sin\theta\cos2\theta + A_9\sin\theta\sin2\theta - A_{10}\cos\theta\cos2\theta + A_{11}\cos\theta\sin2\theta\Big]
\end{aligned}
$$

[9] The kernel expands as $\cot\left(\frac{\varsigma-\theta}{2}\right) = \frac{\sin\theta+\sin\varsigma}{\cos\theta-\cos\varsigma}$.

where the symbols $A_i, i = 1 \ldots 11$ are as in Equations 13 earlier. Again, assuming no flow within the aerofoil, the circumferential velocity is equivalent to the local vorticity.

$$\begin{aligned}\gamma_0(\theta)|_{us} \;=\; \frac{1}{R}\Big[&- A_1 \cos\theta \;-\; \left(A_2 + \tfrac{1}{2}A_7\right)\cos 2\theta \;+\; A_3 \sin\theta \;+\; \left(A_4 - \tfrac{1}{2}A_5 + \tfrac{1}{2}A_6\right)\sin 2\theta \\ &- A_8 \sin\theta\cos 2\theta \;+\; A_9 \sin\theta \sin 2\theta \;-\; A_{10}\cos\theta\cos 2\theta \;+\; A_{11}\cos\theta\sin 2\theta \;+\; \frac{\Gamma_0|_{us}}{2\pi}\Big]\end{aligned} \tag{15}$$

In order to have a finite velocity at the trailing edge, the Kutta-Joukowski condition needs to be enforced there. By setting vorticity $\gamma_0 = 0$ at the trailing edge ($\theta = 0$), the circulation due to the unsteady motion of the aerofoil is found to be

$$\Gamma_0|_{us} = 2\pi\left[2R\left(\dot{l}\sin\alpha + \dot{h}\cos\alpha\right) \;+\; \dot{\alpha}\left(\frac{1}{2}\tau^2 + \frac{1}{2}\sigma^2 - 2R\,(R+a)\right)\right] \tag{16}$$

Combined Quasi-Steady Component

The total effect of the quasi-steady components can be found simply by summing the individual contributions. The total wake-free vorticity distribution is given by the sum of Equations 5 and 15, thus

$$\begin{aligned}\gamma_0(\theta,t) \;=\; \frac{1}{R}\Big[&- A_1 \cos\theta \;-\; \left(A_2 + \tfrac{1}{2}A_7\right)\cos 2\theta \;+\; A_3 \sin\theta \;+\; \left(A_4 - \tfrac{1}{2}A_5 + \tfrac{1}{2}A_6\right)\sin 2\theta \;-\; A_8 \sin\theta\cos 2\theta \\ &+ A_9 \sin\theta \sin 2\theta \;-\; A_{10}\cos\theta\cos 2\theta \;+\; A_{11}\cos\theta\sin 2\theta \;+\; \frac{\Gamma_0(t)}{2\pi}\Big] \;-\; 2U_\infty \sin\left(\theta - \alpha(t)\right)\end{aligned} \tag{17}$$

where the symbols $A_i, i = 1 \ldots 11$ are as in Equation 13 above and where time-dependence has been shown for accuracy. Similarly, by summing Equations 6 and 16, the total quasi-steady wake-free bound circulation is found to be

$$\Gamma_0(t) = 2\pi\left[2R\left((\dot{l}(t) - U_\infty)\sin\alpha(t) + \dot{h}(t)\cos\alpha(t)\right) \;+\; \dot{\alpha}(t)\left(\tfrac{1}{2}\tau^2 + \tfrac{1}{2}\sigma^2 - 2R\,(R+a)\right)\right] \tag{18}$$

Equations 17 and 18, therefore, give the total bound vorticity and circulation, respectively, developed by the aerofoil in the absence of a wake.

3.1.2 Unsteady Component

The unsteady component in the flapping-wing model (see Figure 5) arises from effects induced by the two wakes — the leading-edge vortex (denoted by subscript $_{lv}$) and the trailing-edge wake (denoted by subscript $_{wk}$).

Due to the high angles of attack and the severity of the wing motion during flapping, flow is likely to separate from both the leading and trailing edges of the aerofoil. Therefore, in addition to the conventional wake shed from the trailing edge, a wake is also shed from the leading edge in the form of the leading-edge vortex. The fact that vortex sheets emerge from these points on the aerofoil means that the loading there must be zero, there being none across the vortex sheets. Therefore, the Kutta-Joukowski condition must be satisfied at these points.

The method of images [see e.g. Ref. 78, § 5.1] forms the basis for the analysis in this section. For simplicity, all calculations are performed again in the circle plane. The wakes emanating from the leading and trailing edges of the aerofoil are, therefore, mapped into the circle ($\mathcal{Z}$) plane and may be represented by the schematic in Figure 8. The leading-edge vortices enter the fluid at the leading edge ($\theta = \pi$ on the equivalent circle in the $\mathcal{Z}$-plane) and the trailing-edge vortices make their entry at $\theta = 0$, where θ is measured in the conventional sense. The circle corresponding to the aerofoil has radius R.

For a vortex of strength $\mathrm{d}\Gamma_{wk}$ ($\equiv \gamma_{wk}\mathrm{d}\mathcal{Z}$) at a point $\mathcal{Z}_{wk}$ in the wake, there must exist an (imaginary) image vortex of strength $\mathrm{d}\Gamma_{im_{wk}}$ at the inverse square point[10] in the circle to satisfy the zero-through-flow boundary condition at the surface. The strength and position respectively of this image vortex are given by

$$\mathrm{d}\Gamma_{im_{wk}} = -\mathrm{d}\Gamma_{wk} \qquad \text{and} \qquad \mathcal{Z}_{im_{wk}} = \frac{R^2}{\overline{\mathcal{Z}_{wk}}}$$

where $\overline{\mathcal{Z}_{wk}}$ refers to the complex conjugate of $\mathcal{Z}_{wk}$. By writing the complex potential $\Omega(\mathcal{Z})$ of the system, the velocity at an arbitrary point on the circle $\mathcal{Z}$ ($= R\mathrm{e}^{\imath\theta}$) can be calculated by differentiation w.r.t. $\mathcal{Z}$, to give

$$q(\mathcal{Z}) = \imath\frac{\delta\Gamma_{wk}}{2\pi}\left(\frac{1}{R\mathrm{e}^{\imath\theta} - \overline{\mathcal{Z}_{wk}}} - \frac{\overline{\mathcal{Z}_{wk}}}{R^2 - R\mathrm{e}^{\imath\theta}\overline{\mathcal{Z}_{wk}}}\right)$$

Again using Equation 3, the circumferential velocity is calculated to be

$$v_\theta = -\frac{\delta\Gamma_{wk}}{2\pi R}\Re\left(\frac{\mathcal{Z}_{wk} + R\mathrm{e}^{\imath\theta}}{\mathcal{Z}_{wk} - R\mathrm{e}^{\imath\theta}}\right)$$

from which the circumferential velocity induced by the entire wake can be obtained by integration, thus

$$v_\theta(\theta, t)|_{wk} = -\frac{1}{2\pi R}\oint_{wk}\Re\left(\frac{\mathcal{Z}_{wk} + R\mathrm{e}^{\imath\theta}}{\mathcal{Z}_{wk} - R\mathrm{e}^{\imath\theta}}\right)\gamma_{wk}\,\mathrm{d}\mathcal{Z}_{wk}$$

A similar expression results for the leading-edge vortex so that the combined effect of the two wakes is

$$v_\theta(\theta, t)|_{wk+lv} = -\frac{1}{2\pi R}\oint_{wk}\Re\left(\frac{\mathcal{Z}_{wk} + R\mathrm{e}^{\imath\theta}}{\mathcal{Z}_{wk} - R\mathrm{e}^{\imath\theta}}\right)\gamma_{wk}\,\mathrm{d}\mathcal{Z}_{wk} - \frac{1}{2\pi R}\oint_{lv}\Re\left(\frac{\mathcal{Z}_{lv} + R\mathrm{e}^{\imath\theta}}{\mathcal{Z}_{lv} - R\mathrm{e}^{\imath\theta}}\right)\gamma_{lv}\,\mathrm{d}\mathcal{Z}_{lv} \tag{19}$$

To solve for the two unknown vorticities in the above equation (γ_{wk} and γ_{lv}), two simultaneous 'constraint' equations are required. The equations are provided by satisfying the Kutta-Joukowski condition at the trailing edge of the aerofoil by the addition of circulation and by similarly requiring stagnation at the leading edge. These are derived in turn below.

[10] If two points lie along the same line $\mathrm{e}^{\imath\theta}$, one point outside the circle of radius R at $r_{out}\,\mathrm{e}^{\imath\theta}$ and the other inside it at $r_{in}\,\mathrm{e}^{\imath\theta}$, then the two points lie at inverse square points if $r_{in} \cdot r_{out} = R^2$ [see also Ref. 78, § 5.1].

First Constraint Equation—Kutta-Joukowski Condition at Trailing Edge

In order to enforce the Kutta-Joukowski condition, a circulation Γ_k must be added (as was done previously for the quasi-steady components) so that the circumferential velocity from Equation 19 becomes

$$v_\theta = -\frac{1}{2\pi R}\oint_{wk}\Re\left(\frac{\mathcal{Z}_{wk}+Re^{\imath\theta}}{\mathcal{Z}_{wk}-Re^{\imath\theta}}\right)\gamma_{wk}\,\mathrm{d}\mathcal{Z}_{wk} \;-\; \frac{1}{2\pi R}\oint_{lv}\Re\left(\frac{\mathcal{Z}_{lv}+Re^{\imath\theta}}{\mathcal{Z}_{lv}-Re^{\imath\theta}}\right)\gamma_{lv}\,\mathrm{d}\mathcal{Z}_{lv} \;+\; \frac{\Gamma_k}{2\pi R} \tag{20}$$

To ensure smooth flow at the trailing edge ($\theta = 0$), the Kutta-Joukowski condition ($v_\theta = 0$) is enforced there giving

$$\Gamma_k = \oint_{wk}\Re\left(\frac{\mathcal{Z}_{wk}+R}{\mathcal{Z}_{wk}-R}\right)\gamma_{wk}\,\mathrm{d}\mathcal{Z}_{wk} \;+\; \oint_{lv}\Re\left(\frac{\mathcal{Z}_{lv}+R}{\mathcal{Z}_{lv}-R}\right)\gamma_{lv}\,\mathrm{d}\mathcal{Z}_{lv} \tag{21}$$

Remembering from the method of images that for each vortex outside the circle there exists a vortex of equal but opposite strength inside, Kelvin's law can be applied. Assuming that the initial circulation of the aerofoil-wake-LEV system was zero, we have

$$\Gamma_0(t) + \Gamma_{wk}(t) + \Gamma_{im_{wk}}(t) + \Gamma_{lv}(t) + \Gamma_{im_{lv}} + \Gamma_k(t) = 0$$

from which the following simple result is obtained

$$\Gamma_k(t) = -\Gamma_0(t)$$

Substituting the above into Equation 21 gives the first constraint, thus

$$\Gamma_0(t) = -\left[\oint_{wk}\Re\left(\frac{\mathcal{Z}_{wk}+R}{\mathcal{Z}_{wk}-R}\right)\gamma_{wk}\,\mathrm{d}\mathcal{Z}_{wk} \;+\; \oint_{lv}\Re\left(\frac{\mathcal{Z}_{lv}+R}{\mathcal{Z}_{lv}-R}\right)\gamma_{lv}\,\mathrm{d}\mathcal{Z}_{lv}\right] \tag{22}$$

This is the general wake-integral equation for the flapping-wing problem and is also the circle-plane rendering of a generalised, *nonlinear* form of the original Wagner equation. In his work, Wagner presented a simple, linear form of this equation [45]. Later, von Kármán & Sears obtained the same linear form but using the circulation approach [43, Eqn. 38]). More recently, McCune et al generalised the form of the equation derived by von Kármán & Sears to include the effect of a nonlinear deforming wake [42, 65; see also 67].

The equation presented here (Equation 22) is a further generalisation that is still nonlinear but now includes the effect of a second wake—the leading-edge vortex. This form of the equation has never been presented before and is one of the key novel equations derived in this work.

Second Constraint Equation—Stagnation at Leading Edge

Having enforced the Kutta-Joukowski condition at the trailing edge, the velocity distribution on the circle can be found by summing the wake-free (Equation 17, remembering that velocity and vorticity are interchangeable, i.e. $v_\theta \equiv \gamma_\theta$) and

wake-induced contributions (Equation 20) thus

$$v_\theta = \overbrace{A + \frac{\Gamma_0}{2\pi R}}^{\text{wake-free}} + \underbrace{\left(-\frac{\Gamma_0}{2\pi R}\right) + B}_{\text{wake-induced}} = A + B \tag{23}$$

where

$$A = \frac{1}{R}\Big[- A_1 \cos\theta - \left(A_2 + \tfrac{1}{2}A_7\right)\cos 2\theta + A_3 \sin\theta + \left(A_4 - \tfrac{1}{2}A_5 + \tfrac{1}{2}A_6\right)\sin 2\theta - A_8 \sin\theta\cos 2\theta + A_9 \sin\theta \sin 2\theta - A_{10}\cos\theta\cos 2\theta + A_{11}\cos\theta\sin 2\theta\Big] - 2U_\infty \sin(\theta - \alpha)$$

and

$$B = -\frac{1}{2\pi R}\left[\oint_{wk} \Re\left(\frac{\mathcal{Z}_{wk} + Re^{i\theta}}{\mathcal{Z}_{wk} - Re^{i\theta}}\right)\gamma_{wk}\,\mathrm{d}\mathcal{Z}_{wk} + \oint_{lv} \Re\left(\frac{\mathcal{Z}_{lv} + Re^{i\theta}}{\mathcal{Z}_{lv} - Re^{i\theta}}\right)\gamma_{lv}\,\mathrm{d}\mathcal{Z}_{lv}\right]$$

and where U_∞ is freestream velocity, α is angle of attack and the symbols $A_i, i = 1 \ldots 11$ are as defined in Equation 13.

The leading-edge vortex sheet emanates from the leading edge so that a streamline originating there encloses the leading-edge vortex and reattaches (on most occasions) on the aerofoil further downstream. This implies that there is no load on the wing itself along the leading edge (there being none across the vortex sheet) and, hence, it must be a stagnation point ($v_\theta = 0$). In the circle plane, the leading edge occurs at $\theta = \pi$ so that we have

$$A|_{\theta=\pi} = \frac{1}{R}\left[A_1 - \left(A_2 + \tfrac{1}{2}A_7\right) + A_{10}\right] - 2U_\infty \sin\alpha(t) \tag{24a}$$

and

$$B|_{\theta=\pi} = -\frac{1}{2\pi R}\left[\oint_{wk} \Re\left(\frac{\mathcal{Z}_{wk} - R}{\mathcal{Z}_{wk} + R}\right)\gamma_{wk}\,\mathrm{d}\mathcal{Z}_{wk} + \oint_{lv} \Re\left(\frac{\mathcal{Z}_{lv} - R}{\mathcal{Z}_{lv} + R}\right)\gamma_{lv}\,\mathrm{d}\mathcal{Z}_{lv}\right] \tag{24b}$$

Substituting Equations 24 into Equation 23, equating to zero and rearranging gives

$$\frac{1}{R}\left[A_1 - \left(A_2 + \tfrac{1}{2}A_7\right) + A_{10}\right] - 2U_\infty \sin\alpha(t) = \frac{1}{2\pi R}\left[\oint_{wk} \Re\left(\frac{\mathcal{Z}_{wk} - R}{\mathcal{Z}_{wk} + R}\right)\gamma_{wk}\,\mathrm{d}\mathcal{Z}_{wk} + \oint_{lv} \Re\left(\frac{\mathcal{Z}_{lv} - R}{\mathcal{Z}_{lv} + R}\right)\gamma_{lv}\,\mathrm{d}\mathcal{Z}_{lv}\right] \tag{25}$$

This is the second constraint equation. It expresses the condition for stagnation at the leading edge and is based on the nonlinear wake integral (derived earlier; see Equation 22). This is the second key novel equation derived in the current form for the first time.

Together, Equations 22 and 25 form the cornerstone of the current nonlinear, unsteady, inviscid approach. They are two simultaneous equations that are used to solve for γ_{wk} and γ_{lv} at any point in time t.

In integrating Equations 22 and 25 numerically, the values of previously shed vorticity (γ_{wk} and γ_{lv}) and their respective locations must be known. As will be elaborated in Part II [6], a discrete vortex method is used to implement a solution to these equations and the locations of the vortices serve as the Lagrangian markers $\mathcal{Z}_{wk}$ and $\mathcal{Z}_{lv}$ in the above integral equations. It is, therefore, also necessary to calculate the paths described by these discrete vortices. This is done by implementing vortex convection according to the Rott-Birkhoff equation (see Part II, § 1.1).

Combined Effect of Leading-Edge Vortex and Trailing-Edge Wake

By assuming that there is no flow inside the circle (or aerofoil, for that matter), the surface velocity directly gives the vorticity distribution. By substituting $\Gamma_k(t) = -\Gamma_0(t)$ into Equation 20, the vorticity distribution induced by the leading-edge vortex and the trailing-edge wake vortices on the circle becomes

$$\gamma_1(\theta, t)\big|_{wk+lv} = -\frac{\Gamma_0(t)}{2\pi R} - \frac{1}{2\pi R}\left[\oint_{wk} \Re\left(\frac{\mathcal{Z}_{wk} + Re^{i\theta}}{\mathcal{Z}_{wk} - Re^{i\theta}}\right)\gamma_{wk}\,\mathrm{d}\mathcal{Z}_{wk} + \oint_{lv} \Re\left(\frac{\mathcal{Z}_{lv} + Re^{i\theta}}{\mathcal{Z}_{lv} - Re^{i\theta}}\right)\gamma_{lv}\,\mathrm{d}\mathcal{Z}_{lv}\right] \tag{26}$$

This expression gives the additional bound vorticity induced by the effects of the two shed wakes around the circle.

It may be noted that the above integral equations have all been derived in the circle plane. The form in the aerofoil plane can be obtained by inverting $\mathcal{Z}$ from the mapping in Equation 1 into ζ. This is nontrivial and unnecessary[11].

Equations 18, 22 and 25 together completely define the flapping-wing problem (within the limits of the assumptions made; recall § 2.1.3). For a given set of wing shape and kinematics, the quasi-steady bound circulation $\Gamma_0(t)$ can be computed for all time t using Equation 18. Equations 22 and 25 are then solved simultaneously to compute the circulation shed into the wake. By suitably convecting the shed wake, the solution is updated at each time-step and can also be solved for all time. This process is considered in greater detail in Part II [6].

3.2 Forces and Moments

For a body moving in an incompressible and irrotational flow, two classical methods for calculating the forces and moments on it are found in the literature. The more common approach is to use the unsteady form of the Bernoulli equation

$$\frac{\partial\varphi}{\partial t} + \frac{q^2}{2} + \frac{p}{\rho} + \Pi = f(t) \qquad \text{(a function of time)}$$

where φ is velocity potential, q is velocity, p is pressure, ρ is density and Π is the potential due to extraneous forces on the body (= gz along a streamline, g and z being acceleration due to gravity and height, respectively). This equation is

[11] This is because vorticity (in the circle plane) can be converted easily to circulation (which is the same in both circle and aerofoil planes) using $\Gamma = \oint \gamma\,\mathrm{d}\mathcal{Z}$. See also Equation 2c.

a direct result of the Euler equation. The computation of the $\partial\varphi/\partial t$ term makes the approach cumbersome especially for the flapping wing where perturbations are large and a freestream velocity does not necessarily exist[12]. This approach has, therefore, not been adopted here.

The second method for computing forces and moments is the momentum-based method of vortex pairs used by von Kármán & Sears [43]. The idea is that for every shed vortex, there exists an equal and opposite vortex on the wing and the two constitute a vortex-pair (see Figure 9). The momentum per unit span of the system can be expressed by the sum of the momentum of the vortex-pairs that constitute the system from which force and moment data can then be extracted.

The method was first suggested by Lord Kelvin [81] and has since been discussed by many authors [e.g. 72, 74, 82]. Kelvin showed that for a system of vortices, it is possible to relate the impulse and moment of impulse to the force and moment respectively—so-called *Kelvin's Impulse Theorem*. It may be noted that although the formulation of the above two approaches are quite different, they are both derived from the same Euler equations.

The second method, of vortex pairs, is the approach that has been adopted here. The main advantage is the relative simplicity with which the forces and moments can be computed. The disadvantage, however, is that pressure distributions on the aerofoil surface cannot be computed directly. For the purposes of this study, however, the method is sufficient. The calculation of the forces and moments presented below is in terms of vectors. This is followed by a section dedicated to conversion to complex number notation to tie up with the preceding complex-variable-based unsteady aerodynamic analysis.

3.2.1 Vector Form of Force and Moment Equations

Kelvin's theorem showed that, in the inertial reference frame, the force on the body $\tilde{\boldsymbol{F}}$ is equal to the time rate-of-change of the impulse $\tilde{\boldsymbol{I}}$ of the vortex system, i.e.

$$\tilde{\boldsymbol{F}} = \frac{\mathrm{d}\tilde{\boldsymbol{I}}}{\mathrm{d}t} \qquad \text{where} \quad \tilde{\boldsymbol{I}} = \rho \oiint_S \varphi\, \boldsymbol{n}\, dS \tag{27}$$

where ρ is the fluid density, S is the boundary surface enclosing the body and $\boldsymbol{n}$ is the unit normal vector on the boundary [for detailed derivation, see Ref. 75]. Similarly, the moment of the system about the origin is given by the time rate-of-change of the moment of impulse of the system $\tilde{\boldsymbol{I}}_m$, i.e.

$$\tilde{\boldsymbol{M}} = \frac{\mathrm{d}\tilde{\boldsymbol{I}}_m}{\mathrm{d}t} \qquad \text{where} \quad \tilde{\boldsymbol{I}}_m = \rho \oiint_S \varphi\, (\tilde{\boldsymbol{r}} \wedge \boldsymbol{n})\, \mathrm{d}S \tag{28}$$

[12] For steady flows, Blasius's theorem can also be used to determine the forces (and moments) on a body in a fluid [79, p. 10]. In unsteady flows, however, due to the presence of discontinuities in the wake (from shed vortices) the approach cannot be applied [80, p. 498].

where $\boldsymbol{r}$ is the vector distance from the origin of the coordinate system with respect to which the flow is stationary at infinity. Because this approach is momentum-based, all derivations are made in an inertial coordinate system where Newton's 2nd law of motion is valid. It is, however, more useful to have forces and moments in body-fixed coordinates, and all the more so for a flapping wing. Converting from the inertial ($\tilde{}$) to the body ($\hat{}$) coordinate system (see Figure 6) gives for force [74]

$$\hat{\boldsymbol{F}} = \frac{\mathrm{d}\hat{\boldsymbol{I}}}{\mathrm{d}t} \tag{29}$$

and for moment

$$\hat{\boldsymbol{M}} = \frac{\mathrm{d}\hat{\boldsymbol{I}}_m}{\mathrm{d}t} + \tilde{\boldsymbol{U}} \wedge \hat{\boldsymbol{I}} \tag{30}$$

where $\tilde{\boldsymbol{U}}$ is the translational velocity of the body-fixed system relative to the inertial reference system.

3.2.2 Conversion to Complex Number Form

Due to extensive use of the complex variable in the preceding analysis, it is appropriate to convert the force and moment formulae presented above to complex plane coordinate systems. In this way, force and moment information can be extracted immediately from the calculations without major modifications.

In complex coordinate system notation (ζ-plane), impulse is given by

$$\mathcal{I} = \mathcal{I}_\xi + \imath\mathcal{I}_\eta$$

and force is

$$\mathcal{F} = \mathcal{F}_\xi + \imath\mathcal{F}_\eta \tag{31}$$

where the orthogonal axes are defined by the ξ-η Cartesian system[13]. Moment is a scalar quantity and is given simply by the real number $\mathcal{M}$. It is taken positive counterclockwise (same sense as positive circulation).

Consider two vortices of strengths Γ_1 and Γ_2 at positions $\tilde{\zeta}_1$ and $\tilde{\zeta}_2$ respectively, that constitute a vortex pair[14] in complex space . The impulse of the vortex pair acts perpendicularly and halfway between the two vortices [84, p. 325] so that the complex impulse of the vortex pair is

$$\tilde{\mathcal{I}} = \imath\rho\left(\Gamma_1\tilde{\zeta}_1 + \Gamma_2\tilde{\zeta}_2\right)$$

[13] Alternative notations suggest $\mathcal{F} = \mathcal{F}_\xi - \imath\mathcal{F}_\eta$ where clockwise circulation is taken as positive [83, § 2.3, p. 86]. In our case, positive circulation is counterclockwise.

[14] In the sense described by [43, p. 380]. See also Figure 9.

remembering that $\Gamma_1 = -\Gamma_2$. Calculation of the moment of impulse follows similarly, thus

$$\tilde{I}_m = \frac{\rho}{2}\left(\Gamma_1 \left|\tilde{\zeta}_1\right|^2 + \Gamma_2 \left|\tilde{\zeta}_2\right|^2\right)$$

so that the total impulse and moment of impulse respectively of the entire system are given by

$$\tilde{I} = \imath\rho \sum_{j=1}^{\infty} \Gamma_j \tilde{\zeta}_j \tag{32}$$

$$\tilde{I}_m = \frac{\rho}{2} \sum_{j=1}^{\infty} \Gamma_j \left|\tilde{\zeta}_j\right|^2 \tag{33}$$

If all shed vortices were to lie on the real axis and there were no leading-edge vortices, Equations 32 and 33 would reduce to the form given in the treatment of [43] for a flat (linear) wake.

The force and moment about the origin are found by taking the derivatives w.r.t. time of Equations 32 and 33 (recall Equations 27 and 28), thus

$$\tilde{\mathcal{F}} = \imath\rho \frac{\mathrm{d}}{\mathrm{d}t} \sum_{j=1}^{\infty} \Gamma_j \tilde{\zeta}_j = \imath\rho \frac{\mathrm{d}}{\mathrm{d}t} \int \tilde{\zeta}\, \gamma(\tilde{\zeta})\, \mathrm{d}\tilde{\zeta}$$

$$\tilde{\mathcal{M}} = \frac{\rho}{2} \frac{\mathrm{d}}{\mathrm{d}t} \sum_{j=1}^{\infty} \Gamma_j \left|\tilde{\zeta}_j\right|^2 = \frac{\rho}{2} \frac{\mathrm{d}}{\mathrm{d}t} \int \left|\tilde{\zeta}\right|^2 \gamma(\tilde{\zeta})\, \mathrm{d}\tilde{\zeta}$$

Since the wakes are free vortex sheets, they are incapable of supporting Kutta-Joukowski forces. Any forces on the system are, therefore, sustained only by the bound vortices, i.e. the aerofoil surface. Therefore, computing the forces and moments on the entire system of vortices is equivalent to evaluating forces and moments respectively on the wing.

As mentioned already, it is more useful to have forces and moments in a coordinate system that moves with the aerofoil, in this case the aerofoil-inertia system ($\hat{\xi}$-$\hat{\eta}$ system in Figure 6). Using Equations 29 and 30 then gives

$$\hat{\mathcal{F}} = \frac{\mathrm{d}\hat{I}}{\mathrm{d}t} \tag{34}$$

and

$$\hat{\mathcal{M}} = \frac{\mathrm{d}\hat{I}_m}{\mathrm{d}t} - \Im\left(U_0 \hat{I}\right) \tag{35}$$

where

$$\hat{I} = \imath\rho \sum_{j=1}^{\infty} \Gamma_j \hat{\zeta}_j$$

$$\hat{I}_m = \frac{\rho}{2} \sum_{j=1}^{\infty} \Gamma_j \left|\hat{\zeta}_j\right|^2$$

$$U_0 = \left(-U_\infty + \dot{l}\right) + \imath\dot{h}$$

and U_0 is the translational velocity of the moving system and $\Im$ refers to the 'imaginary part of'.

3.2.3 Components of Forces and Moments

A better understanding of the origin of the forces and moments in the current unsteady aerodynamic model for flapping flight can be achieved by decoupling them into their constituent components. This idea of decomposing the forces and moments goes back to the original work of von Kármán & Sears [43]. Later, McCune et al extended the approach to incorporate the effects of the nonlinear extensions into the forces and moments [65], thereby introducing a further constituent—the deficit due to the deformation of the wake. In the present work, the constituent elements have been further modified from the form given by McCune et al to include the effects of the leading-edge vortices. Such a decomposition is again a novel aspect of this work.

The vorticity in the aerofoil-wake system γ can be decoupled into the aerofoil-bound component γ_a and the shed component γ_s. The bound vorticity term can further be divided into a wake-free component γ_0 and a wake-induced component γ_1. The shed wake can also be divided into a trailing-edge-wake component γ_{wk} and a leading-edge-vortex component γ_{lv}, thus

$$\gamma \;=\; \gamma_a \,+\, \gamma_s \;=\; \gamma_0 \,+\, \gamma_1 \,+\, \gamma_{wk} \,+\, \gamma_{lv}$$

Therefore, from Equation 34 force can be decoupled as

$$\hat{\mathcal{F}} = \imath\rho \left[\frac{\mathrm{d}}{\mathrm{d}t} \int_a \hat{\zeta}\, \gamma_0(\hat{\zeta})\, \mathrm{d}\hat{\zeta} \;+\; \frac{\mathrm{d}}{\mathrm{d}t} \int_a \hat{\zeta}\, \gamma_1(\hat{\zeta})\, \mathrm{d}\hat{\zeta} \;+\; \frac{\mathrm{d}}{\mathrm{d}t} \int_{wk} \hat{\zeta}\, \gamma_{wk}\,(\hat{\zeta})\, \mathrm{d}\hat{\zeta} \;+\; \frac{\mathrm{d}}{\mathrm{d}t} \int_{lv} \hat{\zeta}\, \gamma_{lv}\,(\hat{\zeta})\, \mathrm{d}\hat{\zeta} \right] \tag{37}$$

where the subscript $_a$ means the integral is taken around the aerofoil, and similarly the subscripts $_{wk}$ and $_{lv}$ mean the integral is taken over the respective shed wakes.

For steady motion (aerofoil at a small constant angle of attack in a uniform freestream), the first term above vanishes because the wake-free bound vorticity does not change with time, i.e. $\mathrm{d}\gamma_0/\mathrm{d}t = 0$. The second term also vanishes because the starting vortex is so far away as to have no significant effect on the bound vorticity, i.e. $\gamma_1 \approx 0$. In the absence of a leading-edge vortex (which is reasonable for steady flow at small angle of attack), the only term remaining in Equation 37 is the trailing-edge-wake term. For steady flow, this refers to the starting vortex (of circulation Γ_{wk}). Since this is the only wake vortex, Kelvin's law requires that the bound circulation Γ_0 be equal in strength but of opposite sense. At any time t, the starting vortex is located at $\hat{\zeta}_{wk} = (U_\infty t - l) - \imath h$ so that

$$\begin{aligned} \imath\rho \frac{\mathrm{d}}{\mathrm{d}t} \int_{wk} \gamma_{wk}(\hat{\zeta})\, \hat{\zeta}\, \mathrm{d}\hat{\zeta} \;&=\; \imath\rho\, \Gamma_{wk} \frac{\mathrm{d}}{\mathrm{d}t} \left[(U_\infty t - l) - \imath h \right] \\ &=\; \imath\rho\, \overline{U_0}\, \Gamma_{wk} \end{aligned}$$

where $\overline{U_0}$ refers to the complex conjugate of the incident velocity U_0. This equation yields the classical quasi-steady Kutta-Joukowski lift per unit span because of the equivalence of the bound and starting vortices, i.e. $\imath\rho\overline{U_0}\,\Gamma_{wk} = -\imath\rho\overline{U_0}\,\Gamma_0$.

Forces

Force may, therefore, be decoupled as

$$\hat{\mathcal{F}}(t) = \hat{\mathcal{F}}_0(t) \;+\; \hat{\mathcal{F}}_1(t) \;+\; \hat{\mathcal{F}}_2(t) \;+\; \hat{\mathcal{F}}_3(t) \tag{38}$$

where

$$\begin{aligned}
\hat{\mathcal{F}}_0(t) &= -\imath\rho\overline{U_0}\Gamma_0 \\
\hat{\mathcal{F}}_1(t) &= \imath\rho\frac{\mathrm{d}}{\mathrm{d}t}\int_a \hat{\zeta}\,\gamma_0(\hat{\zeta})\,\mathrm{d}\hat{\zeta} \\
\hat{\mathcal{F}}_2(t) &= \imath\rho\frac{\mathrm{d}}{\mathrm{d}t}\int_a \hat{\zeta}\,\gamma_1(\hat{\zeta})\,\mathrm{d}\hat{\zeta} \\
\hat{\mathcal{F}}_3(t) &= \imath\rho\overline{U_0}\Gamma_0 \;+\; \imath\rho\frac{\mathrm{d}}{\mathrm{d}t}\int_{wk} \hat{\zeta}\,\gamma_{wk}(\hat{\zeta})\,\mathrm{d}\hat{\zeta} \;+\; \imath\rho\frac{\mathrm{d}}{\mathrm{d}t}\int_{lv} \hat{\zeta}\,\gamma_{lv}(\hat{\zeta})\,\mathrm{d}\hat{\zeta}
\end{aligned}$$

Force $\hat{\mathcal{F}}$ is complex-valued and may be written as $\hat{\mathcal{F}} = \hat{\mathcal{F}}_H + \imath\hat{\mathcal{F}}_V$ where $\hat{\mathcal{F}}_H$ and $\hat{\mathcal{F}}_V$ refer to the horizontal and vertical components respectively. For flapping-wing dynamics, the severity of the wing motion makes it difficult to define a mean direction for lift and drag. Therefore, the aerofoil-inertia ($\hat{\xi}$-$\hat{\eta}$) system is used to define lift $\mathcal{L}$ and drag $\mathcal{D}$ as the vertical and horizontal forces[15] (with respect to gravity) respectively, i.e.

$$\hat{\mathcal{F}} = \mathcal{D} + \imath\mathcal{L} \tag{40}$$

From Equation 38, lift and drag may then be written respectively as

$$\mathcal{L}(t) = \mathcal{L}_0(t) + \mathcal{L}_1(t) + \mathcal{L}_2(t) + \mathcal{L}_3(t) \tag{41}$$

$$\mathcal{D}(t) = \mathcal{D}_0(t) + \mathcal{D}_1(t) + \mathcal{D}_2(t) + \mathcal{D}_3(t) \tag{42}$$

In Equation 41, $\mathcal{L}_0$ refers to the quasi-steady contribution to lift—the so-called Kutta-Joukowski lift—that would be achieved in the absence of any wake.

The $\mathcal{L}_1$-term refers to the lift contribution due to apparent-mass effects. In order to allow the wing to pass, fluid must move aside ahead of it and close up after it. This requires kinetic energy which is constant for a wing in uniform flow at constant angle of attack and, hence, there is no net force. However, during wing accelerations there are changes in kinetic

[15] In Part II, reference is also made to thrust $\mathcal{T}$. This is defined as the force parallel to drag but always acting in the direction of wing motion.

energy imparted to the fluid and this manifests in the form of extra or 'added' forces that are termed added or apparent mass. A similar effect would be observed when a wing enters a region of nonuniform flow, e.g. during wake re-entry. Depending on the exact nature of the disturbance, apparent mass could produce either beneficial or detrimental effects.

The $\mathcal{L}_2$-term in Equation 41 represents the lift induced by the presence of the leading-edge vortex and the trailing-edge wake. It is responsible for the Wagner function due to its resistance to any change in flow conditions. In its classical form, it inhibits the growth of bound circulation, and is hence referred to as the lift-deficiency term. The third term ($\mathcal{L}_3$) is of a similar form to that given by Lam [42] but with an additional component due to the leading-edge vortex added. It represents the lift deficit experienced in the presence of the two wakes.

Apparent-mass forces ($\mathcal{L}_1$) arise from impulsive pressures and are, therefore, referred to as *non-circulatory*—they can exist in the absence of circulation (e.g. symmetric flow about a flat plate executing heave oscillations in stationary flow without separation). The rest of the components in Equation 41 ($\mathcal{L}_0, \mathcal{L}_2, \mathcal{L}_3$) are described as *circulatory* since they rely on influencing the bound circulation to affect lift.

The first three terms in Equation 41 have analogues in the classical work of von Kármán & Sears albeit without any nonlinear terms. The fourth term has an analogue in the nonlinear extension described by McCune et al but still without the effect of the leading-edge vortex incorporated. The latter is included in the current work along the lines of the approach for delta wings developed in [67], albeit with appropriate modifications.

Generally, for small-angle perturbations with only trailing-edge separation, the drag component of force is small and usually ignored (except probably in Knoller-Betz investigations, where the propulsive effects of aerofoils oscillating in heave and pitch in freestream flow is exploited). However, in flapping-wing applications with leading-edge separation, this component of force is as significant as lift [26, 60]. The current approach, therefore, provides new insight into the drag analogues of the circulatory and non-circulatory lift components described above (Equation 42).

Although the analysis is inviscid, drag is non-zero. The separated flow on the flapping wing gives rise to a normal force. Since drag is defined here as the horizontal force, a component of the normal force acts in this direction. The method does not, however, account for viscous drag, which might be expected to be a small additional component.

Moments

In a manner similar to that used for forces above, the aerodynamic pitching moment may also be decoupled as

$$\hat{\mathcal{M}} = \frac{\rho}{2}\left[\frac{\mathrm{d}}{\mathrm{d}t}\int_a \left|\hat{\zeta}\right|^2 \gamma_0(\hat{\zeta})\,\mathrm{d}\hat{\zeta} \;+\; \frac{\mathrm{d}}{\mathrm{d}t}\int_a \left|\hat{\zeta}\right|^2 \gamma_1(\hat{\zeta})\,\mathrm{d}\hat{\zeta} \;+\; \frac{\mathrm{d}}{\mathrm{d}t}\int_{wk} \left|\hat{\zeta}\right|^2 \gamma_{wk}(\hat{\zeta})\,\mathrm{d}\hat{\zeta} \;+\; \frac{\mathrm{d}}{\mathrm{d}t}\int_{lv} \left|\hat{\zeta}\right|^2 \gamma_{lv}(\hat{\zeta})\,\mathrm{d}\hat{\zeta}\right]$$
$$- \Im\left[\imath\rho U_0\left(\int_a \hat{\zeta}\,\gamma_0(\hat{\zeta})\,\mathrm{d}\hat{\zeta} \;+\; \int_a \hat{\zeta}\,\gamma_1(\hat{\zeta})\,\mathrm{d}\hat{\zeta} \;+\; \int_{wk} \hat{\zeta}\,\gamma_{wk}\,(\hat{\zeta})\,\mathrm{d}\hat{\zeta} \;+\; \int_{lv} \hat{\zeta}\,\gamma_{lv}\,(\hat{\zeta})\,\mathrm{d}\hat{\zeta}\right)\right]$$

and the constituent component moments are analogously

$$\hat{\mathcal{M}}(t) = \hat{\mathcal{M}}_0(t) \;+\; \hat{\mathcal{M}}_1(t) \;+\; \hat{\mathcal{M}}_2(t) \;+\; \hat{\mathcal{M}}_3(t) \tag{43}$$

where

$$\begin{aligned}
\hat{\mathcal{M}}_0 &= -\Im\left[\imath\rho U_0 \int_a \hat{\zeta}\,\gamma_0(\hat{\zeta})\,\mathrm{d}\hat{\zeta}\right] \\
\hat{\mathcal{M}}_1 &= \frac{\rho}{2}\frac{\mathrm{d}}{\mathrm{d}t}\int_a \left|\hat{\zeta}\right|^2 \gamma_0(\hat{\zeta})\,\mathrm{d}\hat{\zeta} \\
\hat{\mathcal{M}}_2 &= \frac{\rho}{2}\frac{\mathrm{d}}{\mathrm{d}t}\int_a \left|\hat{\zeta}\right|^2 \gamma_1(\hat{\zeta})\,\mathrm{d}\hat{\zeta} - \Im\left[\imath\rho U_0 \int_a \hat{\zeta}\,\gamma_1(\hat{\zeta})\,\mathrm{d}\hat{\zeta}\right] \\
\hat{\mathcal{M}}_3 &= \frac{\rho}{2}\frac{\mathrm{d}}{\mathrm{d}t}\int_{wk} \left|\hat{\zeta}\right|^2 \gamma_{wk}(\hat{\zeta})\,\mathrm{d}\hat{\zeta} - \Im\left[\imath\rho U_0 \int_{wk} \hat{\zeta}\,\gamma_{wk}(\hat{\zeta})\,\mathrm{d}\hat{\zeta}\right] \\
&\quad + \frac{\rho}{2}\frac{\mathrm{d}}{\mathrm{d}t}\int_{lv} \left|\hat{\zeta}\right|^2 \gamma_{lv}(\hat{\zeta})\,\mathrm{d}\hat{\zeta} - \Im\left[\imath\rho U_0 \int_{lv} \hat{\zeta}\,\gamma_{lv}(\hat{\zeta})\,\mathrm{d}\hat{\zeta}\right]
\end{aligned}$$

where $\Im$ denotes the 'imaginary part of' and U_0 is the incident velocity at the origin of the aerofoil-inertia system.

3.3 Extension to Three Dimensions

The approach is extended to three dimensions by using a simple blade-element-type method (strip theory)—the contributions of the individual wing sections are summed to give the total value for the entire wing. The framework is, therefore, essentially a 'quasi-3-D' model with the following assumptions made in the process:

- that there is no mutual interference between adjacent wing sections;
- that there are no 3-D tip vortex effects;
- the effect of a mirror wing on the other side of the FMAV is ignored; and
- that there is no spanwise transport of vorticity in the leading-edge vortex.

These assumptions are inherent in the current modelling framework. There is some experimental justification for the last assumption provided by the work of Dickinson [26, 27, priv. comm.] who observed only weak spanwise flow. Details

of Dickinson's experimental data set are given in Part II [6]. Although not handled here, tip vortex effects may have an important influence [85] (see also, discussion in Part II, § 3.3).

As noted earlier, Sane & Dickinson found remarkable similarity between 2-D and 3-D flapping-wing flow, and strongly speculated on the validity of using simple strip theory to extend 2-D flows to 3-D [56]. The blade-element analogy is, therefore, used here. Use of this method, however, precludes treatment of rapid spanwise changes in wing cross-section.

4 Conclusion

In this work, insect-like flapping-wing flight has been identified as the optimum propulsion method for micro air vehicles designed for indoor use. Hovering is the mode considered here in particular, primarily for its simplicity. Due to the nature of insect wings and their kinematics, the concept of radial chords has been introduced. Using these, radial cross-planes have been defined, which are unwrapped into equivalent flat cross-planes where the 2-D flow is then solved. This allows for easy conversion of the model to 3-D by a blade-element-type analogy.

Insect wings execute a rather complex flapping motion. They flap back and forth while continually changing angle of attack, and rapidly reverse their direction and incidence at the end of each halfstroke. A key feature of such flapping-wing flows is their unsteadiness and the formation of a leading-edge vortex, in addition to the usual wake shed from the trailing edge. What ensues is a complex interaction between the wing and the shed wakes which leads to unsteady oscillating forces and moments.

In our approach, the flow associated with insect-like flapping wings is solved separately in each 2-D cross-plane. It is decomposed into wake-free (quasi-steady) and wake-induced (unsteady) components, and solved individually for each component. By using the linearity property of Laplace's equation, the overall effect is then obtained by linear superposition. The quasi-steady component is determined by accounting for the unsteady motion of the wing and satisfying the Kutta-Joukowski condition at the trailing edge. For the unsteady motion, the shedding of the leading-edge vortex requires the additional requirement to satisfy the Kutta-Joukowski condition at the leading edge. By using Kelvin's law (for the conservation of circulation), two nonlinear wake integral equations are derived. These equations describe the flapping-wing flow in its entirety and form the basis of this work.

Expressions for the forces and moments on the wing have been derived from the method of impulses, mainly for its simplicity. More importantly, these forces (and moments) are decomposed into four constituent elements—quasi-steady, apparent mass, wake-induced and wake components. The current work provides insight into the sources of these

components, especially for drag (which has not been attempted before). In addition, the need for defining lift as the force perpendicular to gravity, as opposed to normal to the relative freestream, for flapping wings has also been established.

Finally, the model is extended to a quasi-3-D one by means of a simple blade-element approach whereby the characteristics for the entire wing are obtained simply by integrating along the span.

The wake-integral equations developed in this work are exact (within the limits of the assumptions made) but do not have a closed analytical form. They must, therefore, be solved by numerical methods. This is the theme, together with validation, of the second part of this paper [6].

The overall modelling approach is summarised in Figure 10. The model requires as input wing geometry and wing kinematics for the hovering flapping wing. These are processed by the nonlinear, unsteady aerodynamic model described above (Equations 18, 22, 25 and 26). The output from the model are force and moment data (via Equations 34 and 35) and flow visualisation (see Part II).

Acknowledgements

The authors are grateful to the EPSRC (through grant numbers GR/M78472/01 and GR/S23025/01) and the UK Ministry of Defence for supporting this work.

REFERENCES

1 **Żbikowski, R.** Flapping Wing Autonomous Micro Air Vehicles: Research Programme Outline. In *Fourteenth International Conference on Unmanned Air Vehicle Systems*, volume Supplementary Papers, pp. 38.1–38.5. 1999.

2 **Żbikowski, R.** Flapping Wing Micro Air Vehicle: A Guided Platform for Microsensors. In *Royal Aeronautical Society Conference on Nanotechnology and Microengineering for Future Guided Weapons*, pp. 1.1–1.11. 1999.

3 **Żbikowski, R.** Flapping Wing Technology. In *European Military Rotorcraft Symposium, Shrivenham, UK, 21-23 March 2000*, pp. 1–7. 2000.

4 **Weis-Fogh, T.** Energetics of Hovering Flight on Hummingbirds and Drosophila. *Journal of Experimental Biology* **56**, pp. 79–104, 1972.

5 **Ansari, S. A.**, **Żbikowski, R.** and **Knowles, K.** A nonlinear unsteady aerodynamic model for insect-like flapping wings in the hover: Part I. Methodology and analysis, 2006. Accepted for publication in IMechE Journal of Aerospace Engineering: Part G.

6 **Ansari, S. A.**, **Żbikowski, R.** and **Knowles, K.** A nonlinear unsteady aerodynamic model for insect-like flapping wings in the hover: Part II. Implementation and validation, 2006. Accepted for publication in IMechE Journal of Aerospace Engineering: Part G.

7 **Ellington, C. P.** The Aerodynamics of Hovering Insect Flight: III. Kinematics. *Philosophical Transactions of the Royal Society of London Series B* **305**, pp. 41–78, 1984.

8 **Ennos, A. R.** The Kinematics and Aerodynamics of the Free Flight of Some Diptera. *Journal of Experimental Biology* **142**, pp. 49–85, 1989.

9 **Dickinson, M. H.**, **Lehmann, F.-O.** and **Sane, S. P.** Wing Rotation and the Aerodynamic Basis of Insect Flight. *Science* **284**, pp. 1954–1960, 18 June 1999.

10 **Ellington, C. P.** The Aerodynamics of Hovering Insect Flight: IV. Aerodynamic Mechanisms. *Philosophical Transactions of the Royal Society of London Series B* **305**, pp. 79–113, 1984.

11 **Ellington, C. P.**, **van den Berg, C.**, **Willmott, A. P.** and **Thomas, A. L. R.** Leading-edge vortices in insect flight. *Nature* **384**, pp. 626–630, 19/26 December 1996.

12 **Willmott, A. P.**, **Ellington, C. P.** and **Thomas, A. L. R.** Flow Visualization and Unsteady Aerodynamics in the Flight of the Hawkmoth, Manduca sexta. *Philosophical Transactions of the Royal Society of London Series B* **352**, pp. 303–316, 1997.

13 **van den Berg, C.** and **Ellington, C. P.** The Three-Dimensional Leading-Edge Vortex of a "Hovering" Model Hawkmoth. *Philosophical Transactions of the Royal Society of London Series B* **352**(1351), pp. 329–340, 29 March 1997.

14 **van den Berg, C.** and **Ellington, C. P.** The Vortex Wake of a "Hovering" Model Hawkmoth. *Philosophical Transactions of the Royal Society of London Series B* **352**(1351), pp. 317–328, 29 March 1997.

15 **Martin, L. J.** and **Carpenter, P. W.** Flow-visualisation experiments on butterflies in simulated gliding flight. *Fortschritte der Zoologie* **24**(2/3), pp. 307–316, 1977.

16 **Maxworthy, T.** Experiments on the Weis-Fogh Mechanism of Lift Generation by Insects in Hovering Flight. Part 1: Dynamics of the 'fling'. *Journal of Fluid Mechanics* **93**, pp. 47–63, 1979.

17 **Brodsky, A. K.** Vortex Formation in the Tethered Flight of the Peacock Butterfly Inachis Io L. (Lepidoptera, Nymphalidae) and Some Aspects of Insect Flight Evolution. *Journal of Experimental Biology* **161**, pp. 77–95, 1991.

18 Dickinson, M. H. and **Götz, K. G.** Unsteady Aerodynamic Performance of Model Wings at Low Reynolds Numbers. *Journal of Experimental Biology* **174**, pp. 45–64, 1993.

19 Sunada, S., **Kawachi, K.**, **Watanabe, I.** and **Azuma, A.** Performance of a Butterfly in Take-Off Flight. *Journal of Experimental Biology* **183**, pp. 249–277, 1993.

20 Ellington, C. P. Unsteady Aerodynamics of Insect Flight. *The Society for Experimental Biology* pp. 109–129, 1995.

21 Dickinson, M. H. Unsteady Mechanisms of Force Generation in Aquatic and Aerial Locomotion. *Amer. Zool.* **36**, pp. 537–554, 1996.

22 Żbikowski, R. On aerodynamic modelling of an insect-like flapping wing in hover for micro air vehicles. *Philosophical Transactions of the Royal Society of London Series A* **360**, pp. 273–290, 2002.

23 McCroskey, W. J. The Phenomenon of Dynamic Stall. Technical Memorandum TM-81264, NASA, 1981. Pp.1–31.

24 Dickinson, M. Solving the Mystery of Insect Flight. *Scientific American* pp. 34–41, June 2001.

25 Liu, H., **Ellington, C. P.**, **Kawachi, K.**, **van den Berg, C.** and **Wilmott, A. P.** A Computational Fluid Dynamic Study of Hawkmoth Hovering. *Journal of Experimental Biology* **201**, pp. 461–477, 1998.

26 Birch, J. M. and **Dickinson, M. H.** Spanwise Flow and the Attachment of the Leading-Edge Vortex on Insect Wings. *Nature* **412**(6848), pp. 729–733, 2001.

27 Sane, S. P. and **Dickinson, M. H.** The Control and Flight Force by a Flapping Wing: Lift and Drag Production. *Journal of Experimental Biology* **204**, pp. 2607–2626, 2001.

28 Dickinson, M. H. The Effects of Wing Rotation on Unsteady Aerodynamic Performance at Low Reynolds Numbers. *Journal of Experimental Biology* **192**, pp. 179–206, 1994.

29 Sane, S. P. The aerodynamics of insect flight. *Journal of Experimental Biology* **206**(23), pp. 4191–4208, December 2003.

30 Rozhdestvensky, K. V. and **Ryzhov, V. A.** Aerohydrodynamics of flapping-wing propulsors. *Progress in Aerospace Sciences* **39**(8), pp. 585–633, November 2003.

31 Lehmann, F. O. The mechanisms of lift enhancement in insect flight. *Naturwissenschaften* **91**(3), pp. 101–122, March 2004.

32 Osborne, M. F. M. Aerodynamics of Flapping Flight with Application to Insects. *Journal of Experimental Biology* **28**, pp. 221–245, 1951.

33 Pringle, J. W. S. *Insect Flight*, volume 52 of *Oxford Biology Readers*. Oxford University Press, Glasgow, 1975.

34 Weis-Fogh, T. Quick Estimates of Flight Fitness in Hovering Animals, Including Novel Mechanisms for Lift Production. *Journal of Experimental Biology* **59**, pp. 169–230, 1973.

35 Ellington, C. P. The Aerodynamics of Hovering Insect Flight: I. The Quasi-Steady Analysis. *Philosophical Transactions of the Royal Society of London Series B* **305**, pp. 1–15, 1984.

36 Ellington, C. P. The Aerodynamics of Hovering Insect Flight: II. Morphological Parameters. *Philosophical Transactions of the Royal Society of London Series B* **305**, pp. 17–40, 1984.

37 Ellington, C. P. The Aerodynamics of Hovering Insect Flight: V. A Vortex Theory. *Philosophical Transactions of the Royal Society of London Series B* **305**, pp. 115–144, 1984.

38 Ellington, C. P. The Aerodynamics of Hovering Insect Flight: VI. Lift and Power Requirements. *Philosophical Transactions of the Royal Society of London Series B* **305**, pp. 145–181, 1984.

39 Scott, M. T. Nonlinear Airfoil-Wake Interaction in Large Amplitude Unsteady Flow. Master's thesis, Massachusetts Institute of Technology, August 1987.

40 van der Wall, B. G. and **Leishman, J. G.** On the Influence of Time-Varying Flow Velocity on Unsteady Aerodynamics. *Journal of the American Helicopter Society* **39**(4), pp. 25–36, 1994.

41 Benson, H. A. O. Apparent-Mass and On-Board Circulation of Joukowski Airfoils and Cascades in Severe Unsteady Motion. Master's thesis, Massachusetts Institute of Technology, May 1989.

42 Lam, C.-M. G. Nonlinear Wake Evolution of Joukowski Aerofoils in Severe Maneuver. Master's thesis, Massachusetts Institute of Technology, June 1989.

43 von Kármán, T. and **Sears, W. R.** Airfoil Theory for Non-Uniform Motion. *Journal of the Aeronautical Sciences* **5**(10), pp. 379–390, August 1938.

44 Pedersen, C. B. An indicial-Polhamus model of aerodynamics of insect-like flapping wings in hover. Ph.D. thesis, Cranfield University (RMCS Shrivenham), 17 June 2003.

45 Wagner, H. Über die Entstehung des Dynamischen Aufftriebes von Tragflügeln. *Zeitschrift für Angewandie Mathematik und Mechanik* **5**(1), pp. 17–35, February 1925. (On the Occurrence of Dynamic Lift of Wings).

46 Theodorsen, T. General Theory of Aerodynamic Instability and the Mechanism of Flutter. Report 496, NACA, 1935. Pp.413–433.

47 Loewy, R. G. A Two-Dimensional Approximation to the Unsteady Aerodynamics of Rotary Wings. *Journal of the Aeronautical Sciences* pp. 81–93, February 1957. Vertol Aircraft Corporation.

48 Polhamus, E. C. A Concept of the Vortex Lift of Sharp-Edge Delta Wings Based on a Leading-Edge Suction Analogy. Technical Note TN D-3767, NASA, December 1966. 1–15.

49 Minotti, F. O. Unsteady two-dimensional theory of a flapping wing. *Physical Review E* **66**(051907), pp. 1–10, 2002.

50 Graham, J. M. R. The lift on an aerofoil in starting flow. *Journal of Fluid Mechanics* **133**, pp. 413–425, 1983.

51 Jones, K. D., **Dohring, C. M.** and **Platzer, M. F.** Wake Structures Behind Plunging Airfoils: A Comparison of Numerical and Experimental Results. In *34th Aerospace Sciences Meeting & Exhibit*, AIAA-96-0078, pp. 1–9. AIAA, January 1996. January.

52 Jones, K. D. and **Platzer, M. F.** Numerical Computation of Flapping-Wing Propulsion and Power Extraction. In *35th Aerospace Sciences Meeting & Exhibit*, AIAA-97-0826, pp. 1–16. AIAA, January 1997. January.

53 Jones, K. D. and **Platzer, M. F.** An Experimental and Numerical Investigation of Flapping-Wing Propulsion. In *37th Aerospace Sciences Meeting & Exhibit*, AIAA-99-0995, pp. 1–13. AIAA, January 1999. January.

54 Jones, K. D. and **Platzer, M. F.** Flapping-Wing Propulsion for a Micro Air Vehicle. In *38th Aerospace Sciences Meeting & Exhibit*, AIAA-2000-0897, pp. 1–13. AIAA, January 2000. January.

55 Jones, K., **Duggan, S.** and **Platzer, M.** Flapping-Wing Propulsion for a Micro Air Vehicle. In *39th Aerospace Sciences Meeting & Exhibit*, AIAA-2001-0126, pp. 1–14. AIAA, January 2001. January.

56 Sane, S. P. and **Dickinson, M. H.** The aerodynamic effects of wing rotation and a revised quasi-steady model of flapping flight. *Journal of Experimental Biology* **205**, pp. 1087–1096, 2002.

57 Wang, Z. J. Two Dimensional Mechanism for Insect Hovering. *Physics Review Letters* **85**(10), pp. 2216–2219, 4 September 2000.

58 Wang, Z. J. Dissecting Insect Flight. *Annual Review of Fluid Mechanics* **37**, pp. 183–210, 2005.

59 Wang, Z. J. Vortex shedding and frequency selection in flapping flight. *Journal of Fluid Mechanics* **410**, pp. 323–341, 2000.

60 Wang, Z. J. Using Drag to Hover. *arXiv* (physics/0304069 v1), pp. 1–12, 18 April 2003. `http://arxiv.org/PS_cache/physics/pdf/0304/0304069.pdf`.

61 Pullin, D. I. and **Wang, Z. J.** Unsteady forces on an accelerating plate and application to hovering insect flight. *Journal of Fluid Mechanics* **509**, pp. 1–21, 2004.

62 Jones, M. A. The separated flow of an inviscid fluid around a moving flat plate. *Journal of Fluid Mechanics* **496**, pp. 405–441, 2003.

63 Zdunich, P. A Discrete Vortex Model of Unsteady Separated Flow About a Thin Aerofoil for Application to Hovering Flapping-Wing Flight. Master's thesis, University of Toronto, 2002.

64 Thwaites, B. (editor). *Incompressible Aerodynamics: An Account of the Theory and Observation of the Steady Flow of Incompressible Fluid past Aerofoils, Wings, and Other Bodies*. Fluid Motion Memoirs. Oxford University Press, 1960.

65 McCune, J. E., **Lam, C.-M. G.** and **Scott, M. T.** Nonlinear Aerodynamics of Two-Dimensional Airfoils in Severe Maneuver. *AIAA Journal* **28**(3), pp. 385–393, March 1990.

66 McCune, J. E. and **Tavares, T. S.** Perspective: Unsteady wing theory – the Kármán/Sears legacy. *Transactions of the ASME: Journal of Fluids Engineering* **115**(4), pp. 548–560, 1993.

67 Tavares, T. S. and **McCune, J. E.** Aerodynamics of Maneuvering Slender Wings with Leading-Separation. *AIAA Journal* **31**(6), pp. 977–986, June 1993.

68 Wakeling, J. M. and **Ellington, C. P.** Dragonfly Flight: II. Velocities, Accelerations and Kinematics of Flapping Flight. *Journal of Experimental Biology* **200**, pp. 557–582, 1997.

69 Lipschutz, M. M. *Differential Geometry*. Schaum's Outline Series. McGraw-Hill Publishing Company, 1969.

70 Brown, C. E. and **Michael, W. H.** Effect of Leading-Edge Separation on the Lift of a Delta Wing. *Journal of the Aeronautical Sciences* **21**(10), pp. 690–694 & 706, Oct 1954. Also appeared as [86].

71 Katz, J. and **Plotkin, A.** *Low-Speed Aerodynamics*. Cambridge Univeristy Press, second edition, 2001.

72 Lamb, S. H. *Hydrodynamics*. Cambridge University Press, sixth edition, 1932.

73 Glauert, H. *The Elements of Aerofoil and Airscrew Theory*. Cambridge University Press, second edition, 1959.

74 Karamcheti, K. *Principles of Ideal-Fluid Aerodynamics*. Krieger Publishing Company, 1966.

75 Ansari, S. A. A Nonlinear, Unsteady, Aerodynamic Model for Insect-like Flapping Wings in the Hover with Micro Air Vehicle Applications. Ph.D. thesis, Cranfield University (RMCS Shrivenham), September 2004.

76 Smith, M. J. C., **Wilkin, P. J.** and **Williams, M. H.** The Advantages of an Unsteady Panel Method in Modelling the Aerodynamic Forces on Rigid Flapping Wings. *Journal of Experimental Biology* **199**, pp. 1073–1083, 1996.

77 von Helmholtz, H. On Integrals of the Hydrodynamic Equations which express Vortex Motion. *Philosophical Magazine* **4**, pp. 485–512, 1858. (Translation by P. G. Tait, 1867).

78 Milne-Thomson, L. M. *Theoretical Aerodynamics*. Dover, fourth edition, 1966.

79 Blasius, H. Funktionentheoretische Methoden in der Hydrodynamik. *Z. agnew. Math. Mech.* **58**, 1910.

80 Panton, R. L. *Incompressible Flow*. John Wiley & Sons, second edition, 1996.

81 Thomson, W. On Vortex Motion. In *Mathematical and Physical Papers: Volume IV Hydrodynamics and General Dynamics*. Cambridge University Press, 1910. A.k.a. Lord Kelvin.

82 Wu, J. C. Theory for Aerodynamic Force and Moment in Viscous Flow. *AIAA Journal* **19**(4), pp. 434–441, Apr 1981.

83 Robinson, A. and **Laurmann, J. A.** *Wing Theory*. Cambridge University Press, 1956.

84 Durand, W. F. (editor). *Aerodynamic Theory: A General Review of Progress – Vol. II*. Julius Springer, 1935.

85 Ramasamy, M., **Leishman, J. G.** and **Singh, B.** Wake Structure Diagnostics of a Flapping Wing MAV. In *SAE International Powered Lift Conference*, IPLC 2005-01-3198. Texas, 3–6 October 2005.

86 Brown, C. E. and **Michael, W. H.** On Slender Delta Wings with Leading-Edge Separation. Technical Report TN 3430, NACA, 1955. Also appeared as [70].

List of Figures

1 Top view of insect flapping. Note that the leading edge (thick line) always leads 43

2 Wing tip path of an insect tracing a figure-of-eight profile 44

3 Radial chord representation of a fruit fly wing 45

4 Radial and flat cross-planes showing inertial ($\tilde{\xi}, \tilde{\eta}$) and aerofoil ($\xi, \eta$) coordinate systems 46

5 Flapping wing aerodynamic model components. 'Quasi-steady' components refer to the wake-free contributions and 'unsteady' components refer to the wake-induced contribution 47

6 Coordinate systems 48

7 Wing at an angle of attack α in a constant freestream U_∞ 49

8 Wake systems 50

9 2-D vortex ring [after Ref. 43] 51

10 Data flow in the current aerodynamic model 52

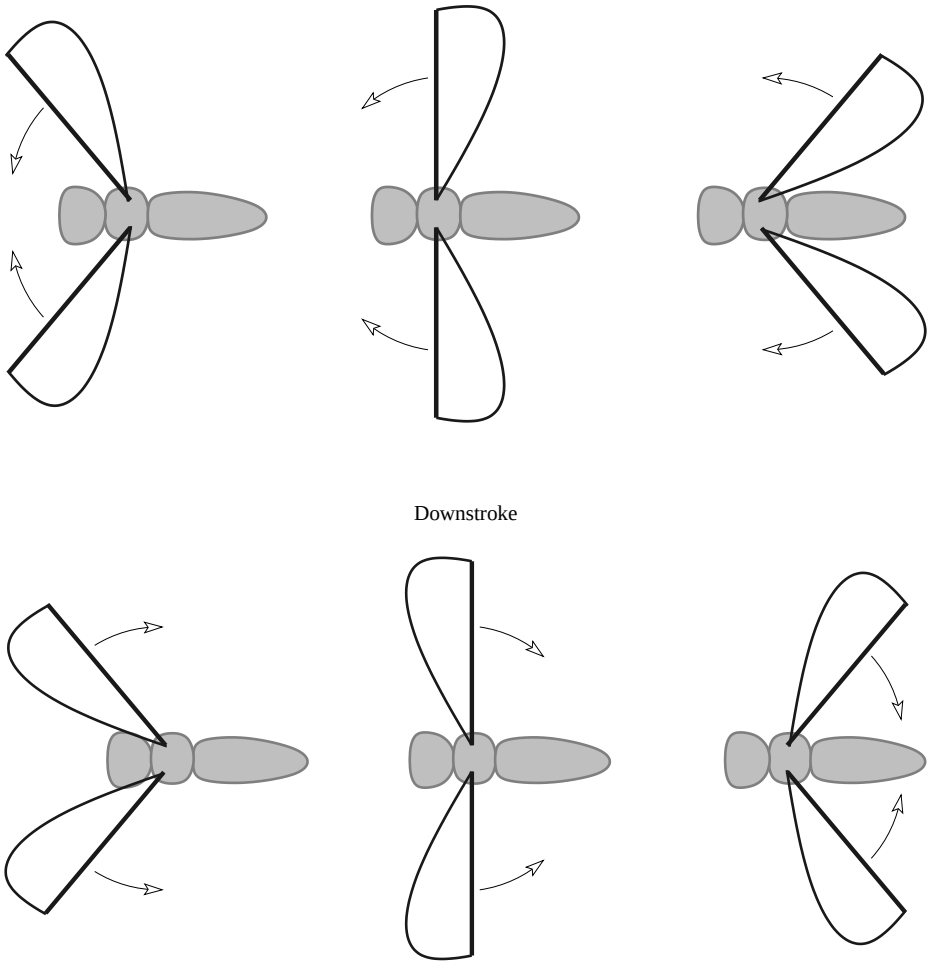

Figure 1: Top view of insect flapping. Note that the leading edge (thick line) always leads

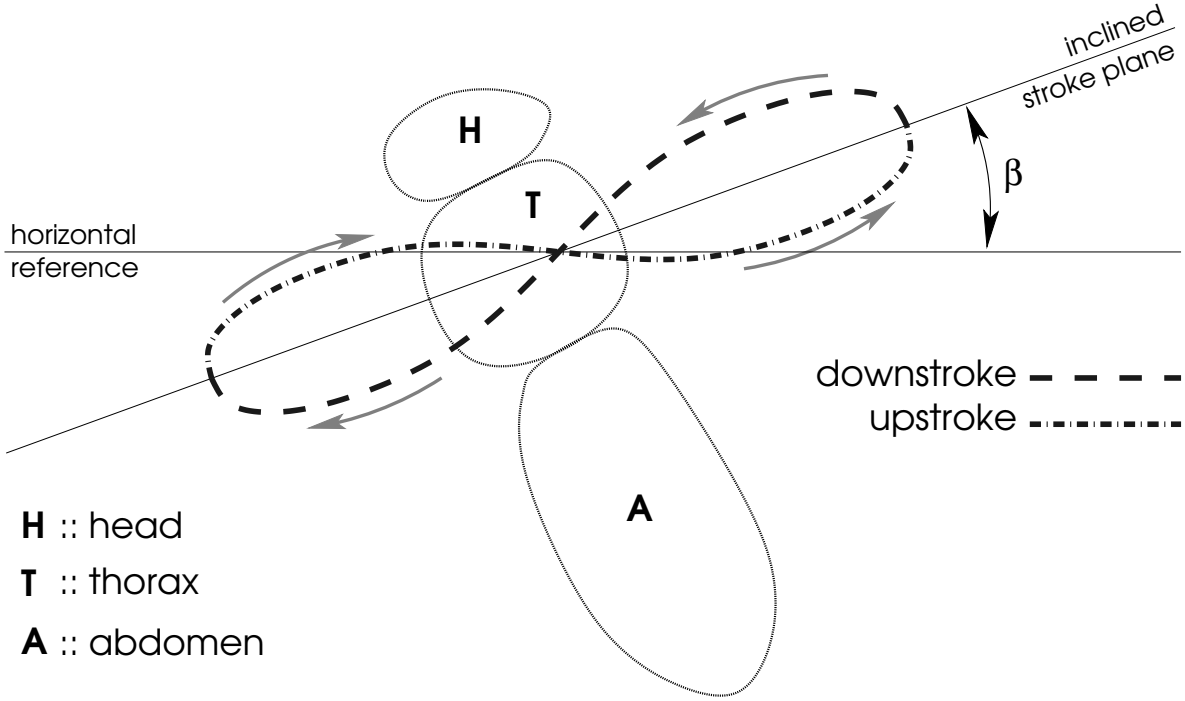

Figure 2: Wing tip path of an insect tracing a figure-of-eight profile

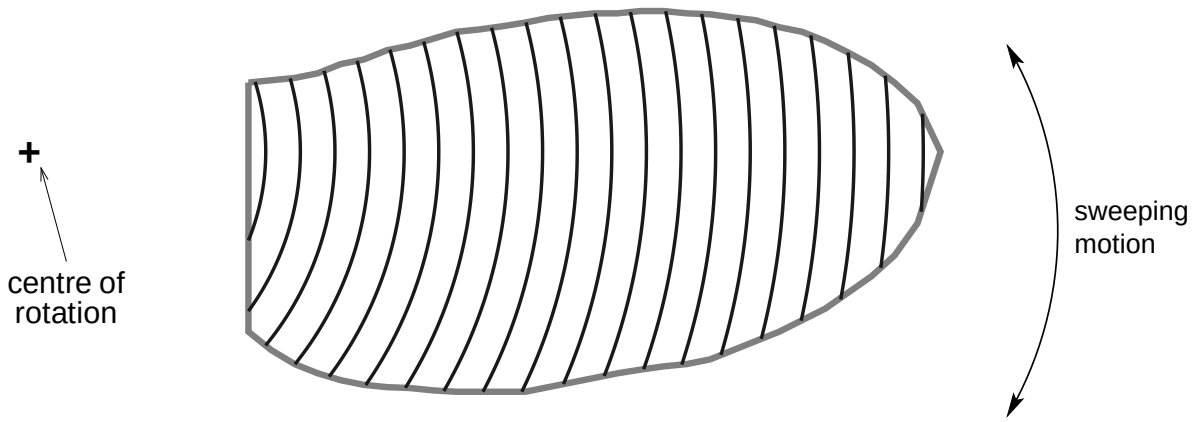

Figure 3: Radial chord representation of a fruit fly wing

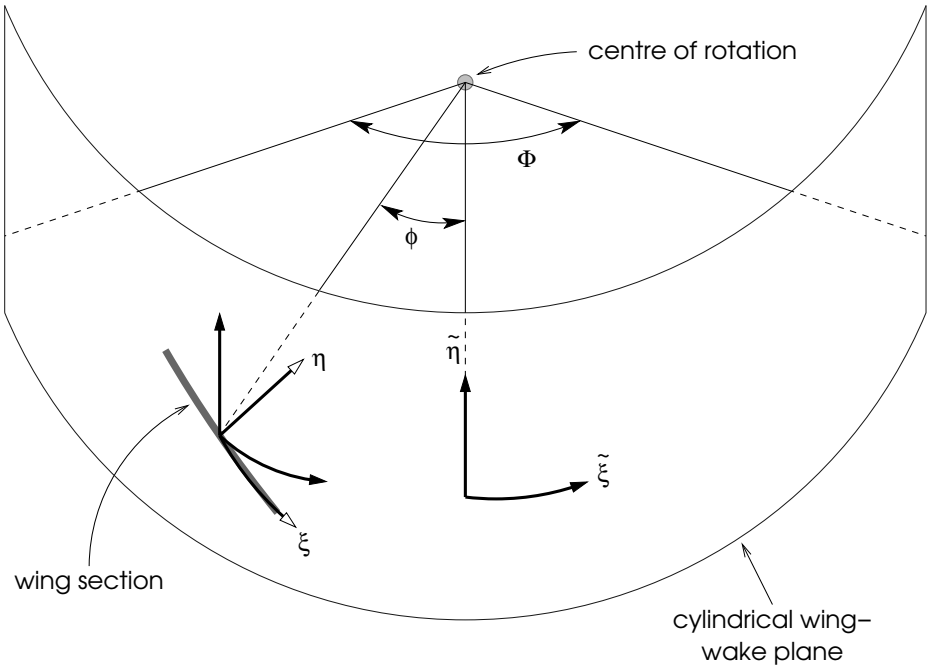

(a) Actual radial cross-plane

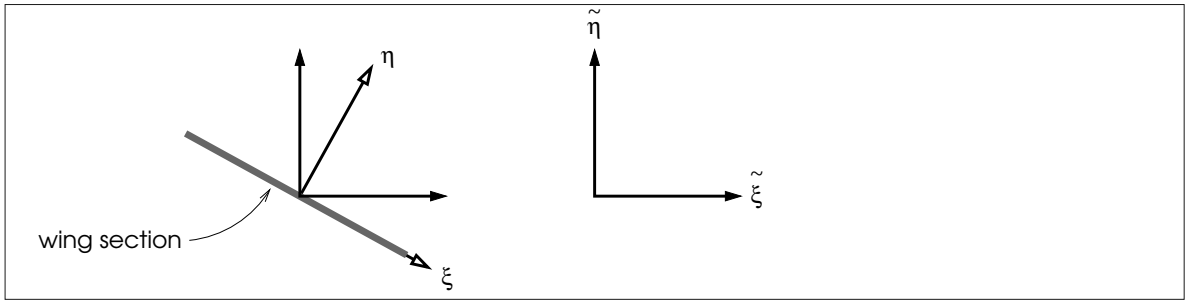

(b) Equivalent flat cross-plane

Figure 4: Radial and flat cross-planes showing inertial $(\tilde{\xi}, \tilde{\eta})$ and aerofoil (ξ, η) coordinate systems

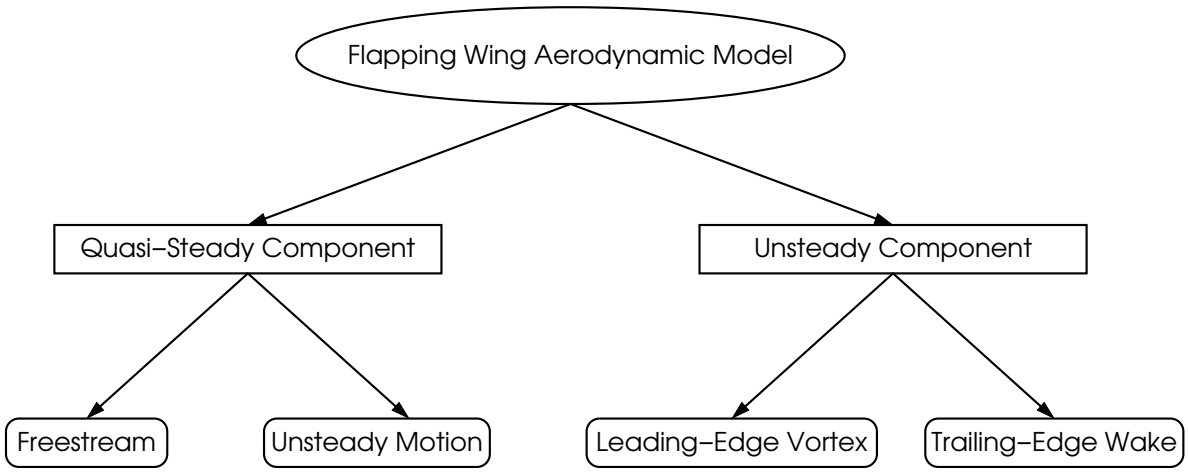

Figure 5: Flapping wing aerodynamic model components. ‘Quasi-steady’ components refer to the wake-free contributions and ‘unsteady’ components refer to the wake-induced contribution

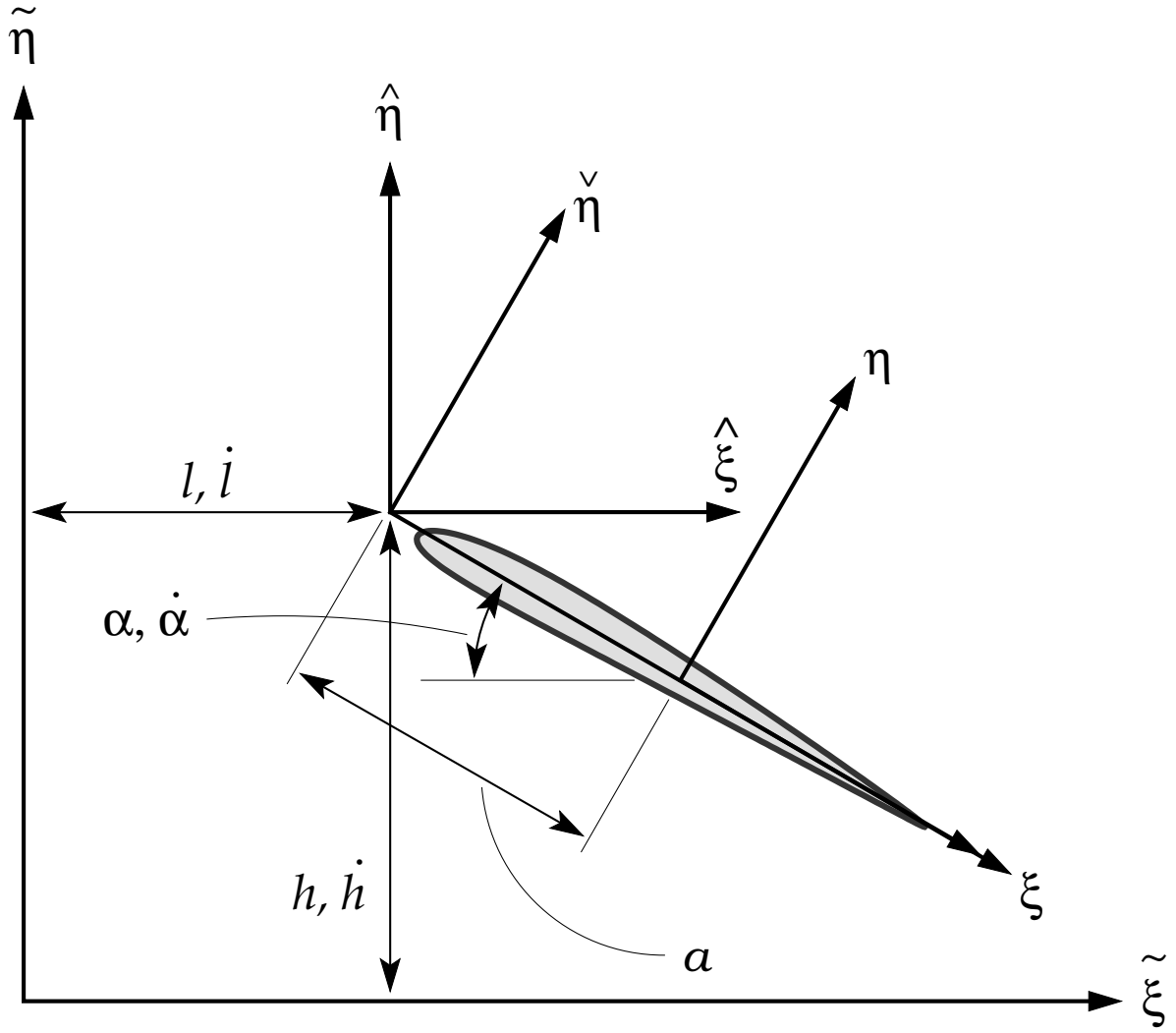

Figure 6: Coordinate systems

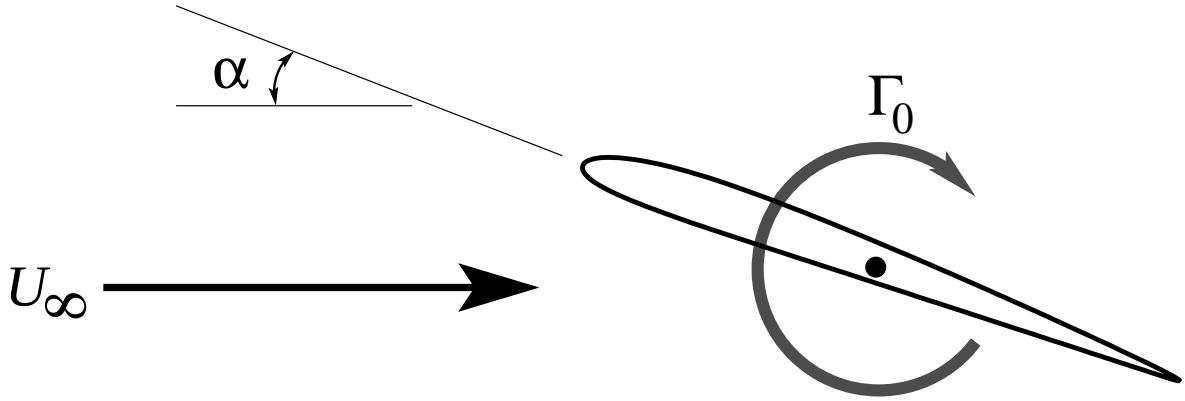

Figure 7: Wing at an angle of attack α in a constant freestream U_∞

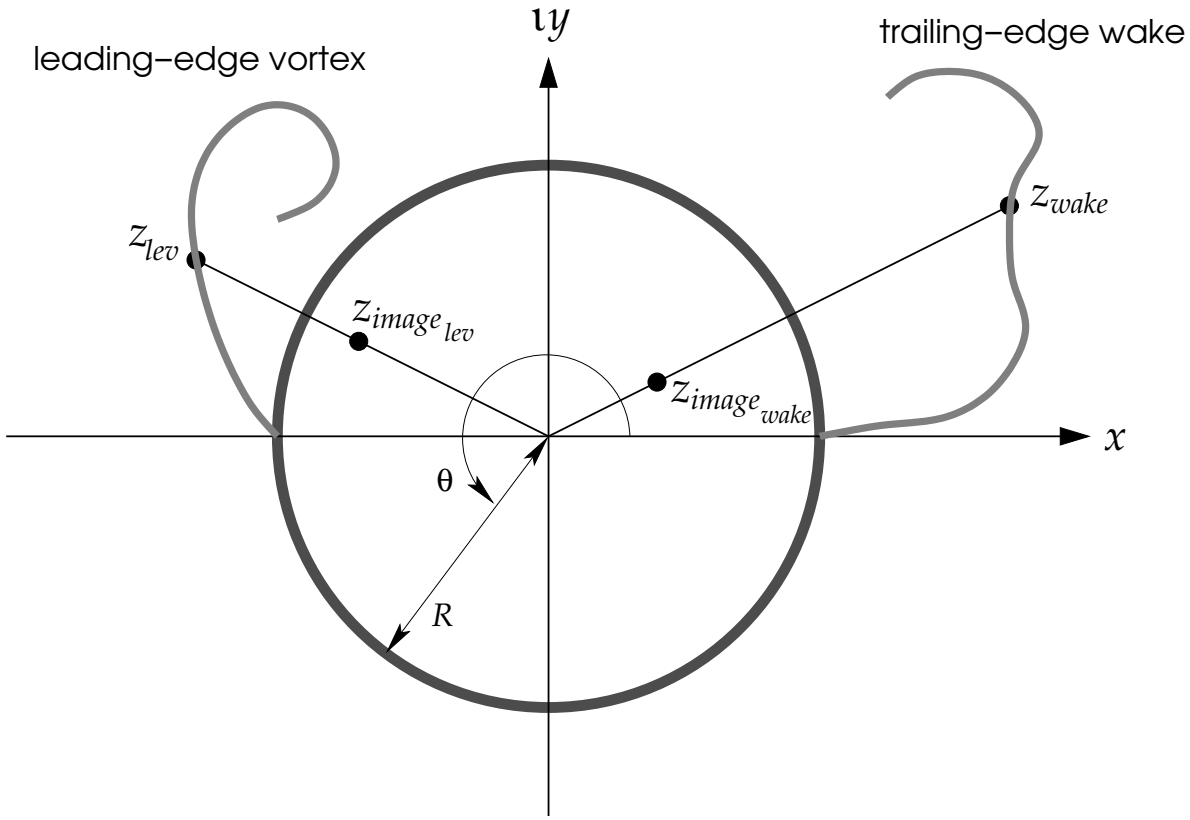

Figure 8: Wake systems

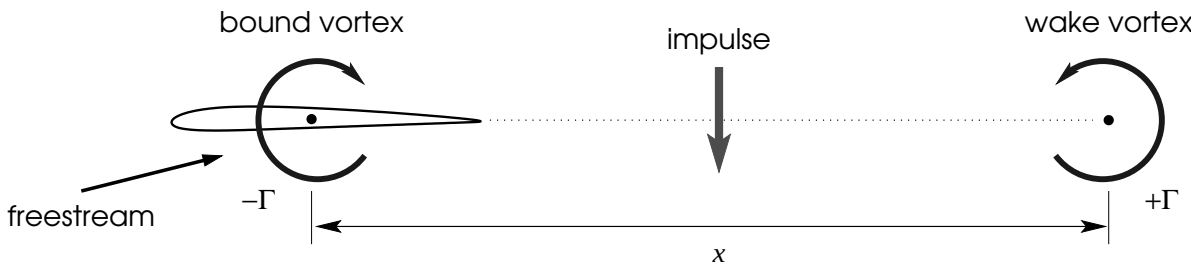

Figure 9: 2-D vortex ring [after Ref. 43]

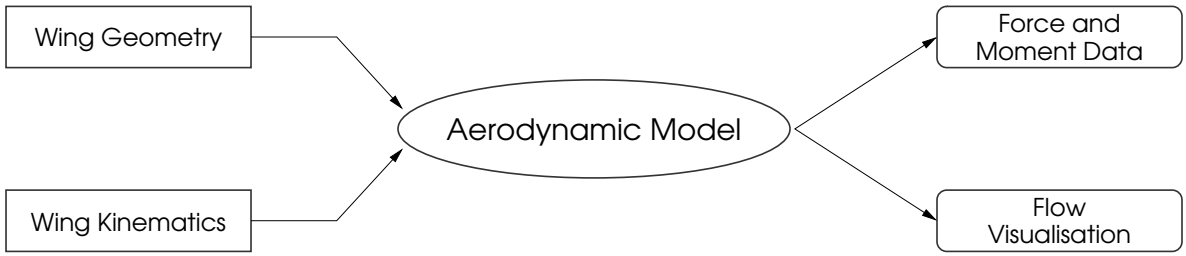

Figure 10: Data flow in the current aerodynamic model